US 20240167874A1

(19) **United States**
(12) **Patent Application Publication** (10) **Pub. No.: US 2024/0167874 A1**
Lawrence (43) **Pub. Date: May 23, 2024**

(54) **PIXEL SCALE FABRY PEROT FILTER ARRAY FOR CHEMICAL AGENT VAPOR DETECTION**

(71) Applicant: **Massachusetts Institute of Technology**, Cambridge, MA (US)

(72) Inventor: **William Lawrence**, Medford, MA (US)

(73) Assignee: **Massachusetts Institute of Technology**, Cambridge, MA (US)

(21) Appl. No.: **18/159,385**

(22) Filed: **Jan. 25, 2023**

Related U.S. Application Data

(60) Provisional application No. 63/324,561, filed on Mar. 28, 2022.

Publication Classification

(51) **Int. Cl.**
G01J 3/28 (2006.01)
G01J 3/02 (2006.01)
G03F 7/00 (2006.01)

(52) **U.S. Cl.**
CPC ***G01J 3/2803*** (2013.01); ***G01J 3/021*** (2013.01); ***G03F 7/0007*** (2013.01); *G01J 2003/2806* (2013.01)

(57) **ABSTRACT**

Fabry-Pérot filters having different cavity thicknesses are formed in arrays on a substrate for spectral sensing. The filter array can be coupled to a detector array to make a compact, low size, weight and power spectral sensor that detects spectral information in a scene viewed by the detector array. The spectral sensor can be used in a compact spectrometer to detect the presence of harmful chemical vapors.

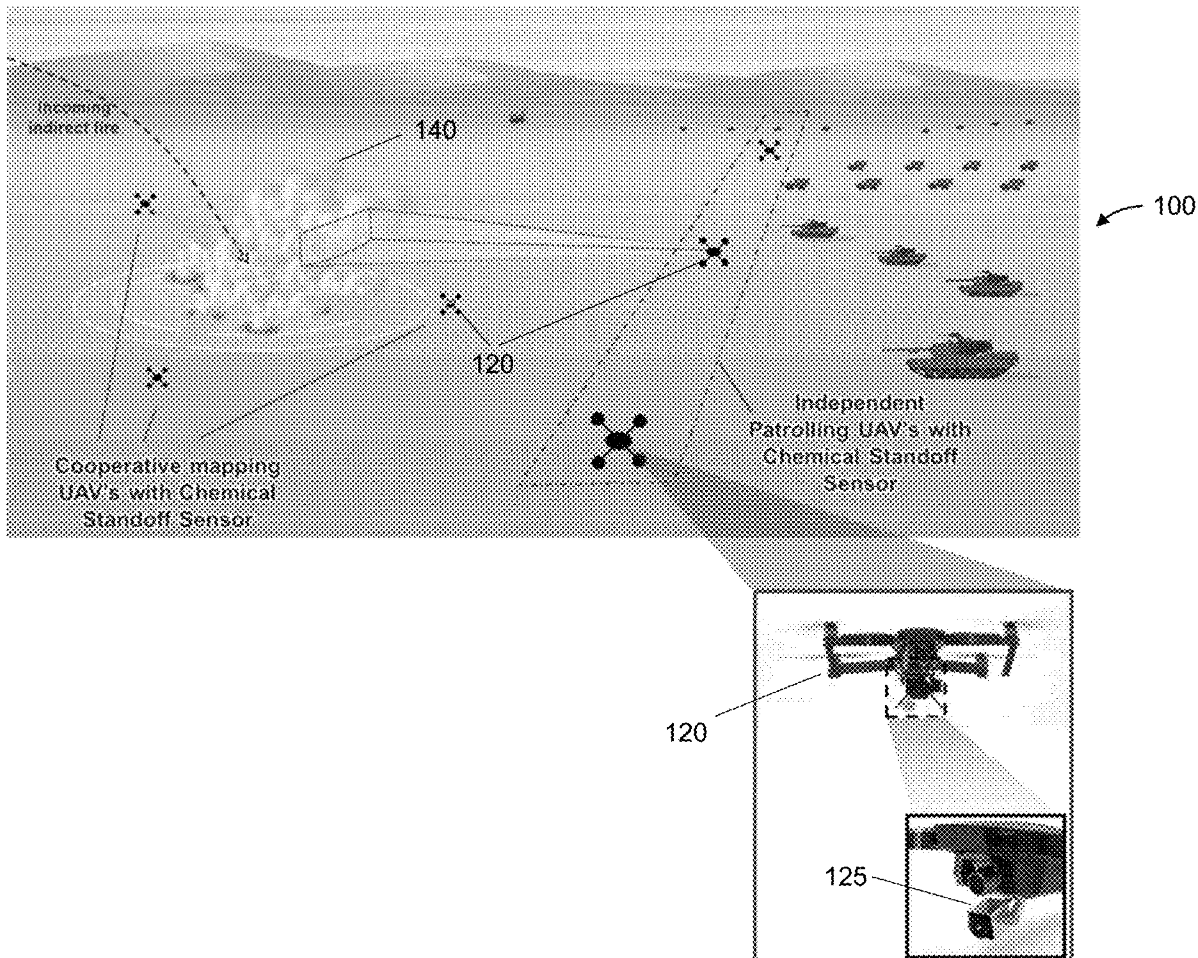

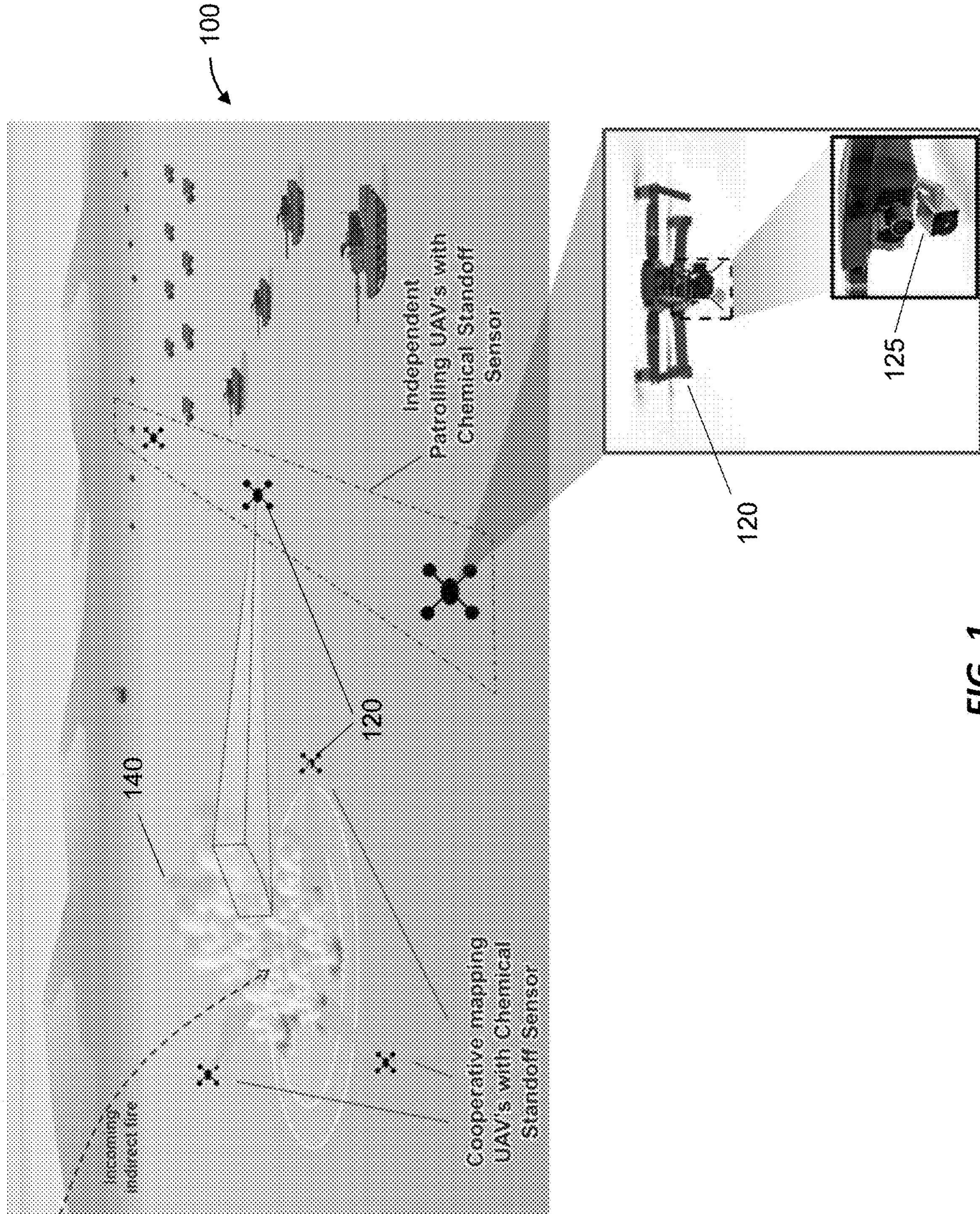

FIG. 1

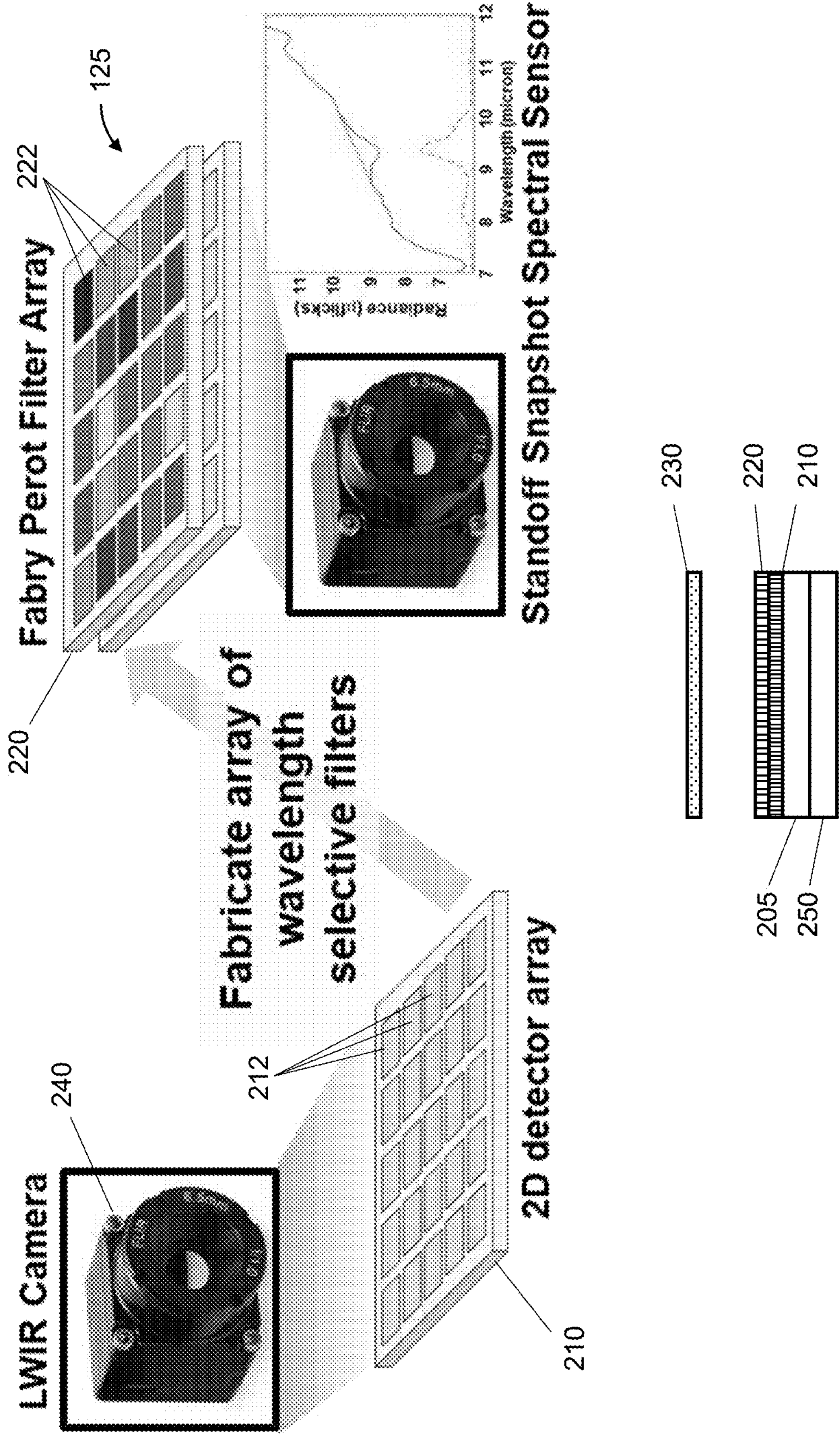

FIG. 2

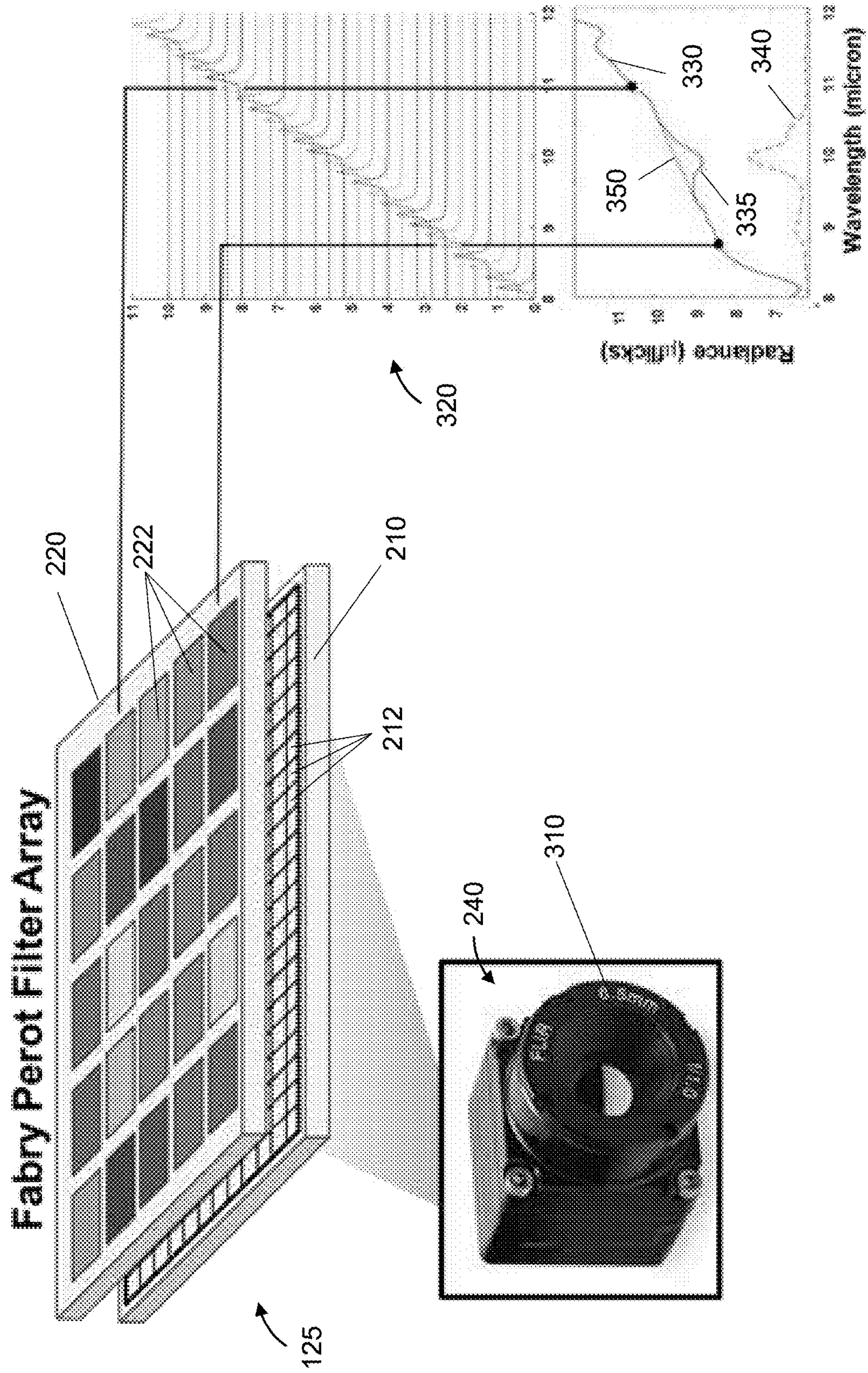

FIG. 3

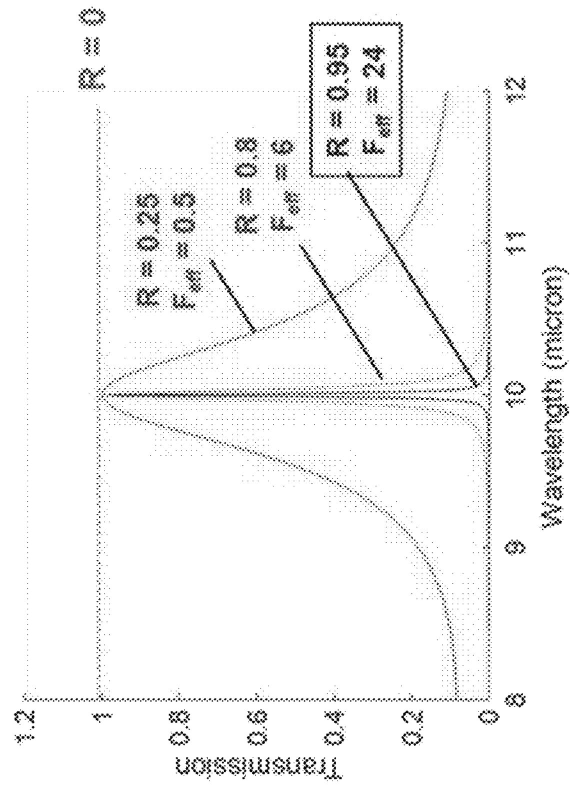

FIG. 5

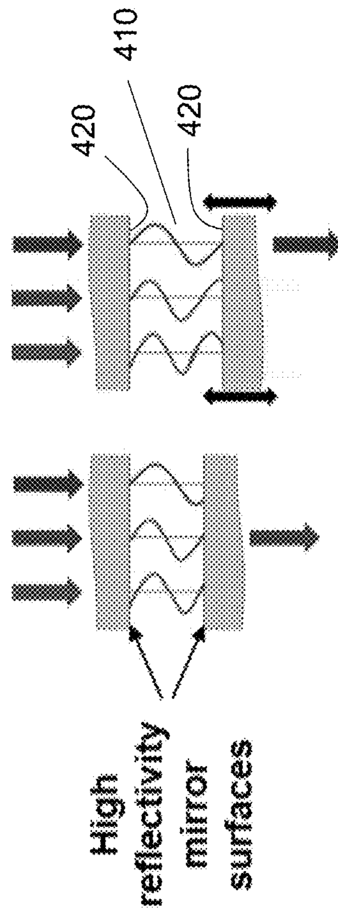

FIG. 4

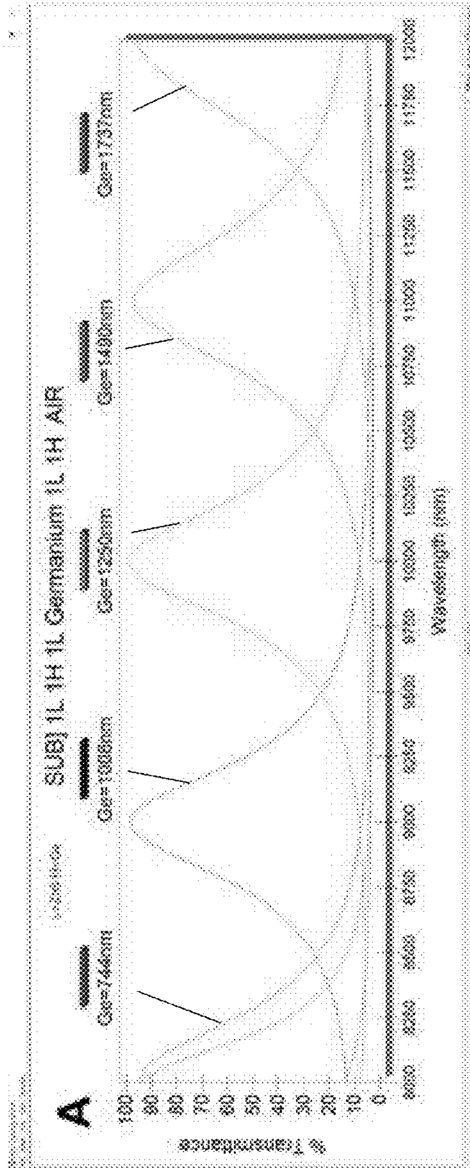

FIG. 6A

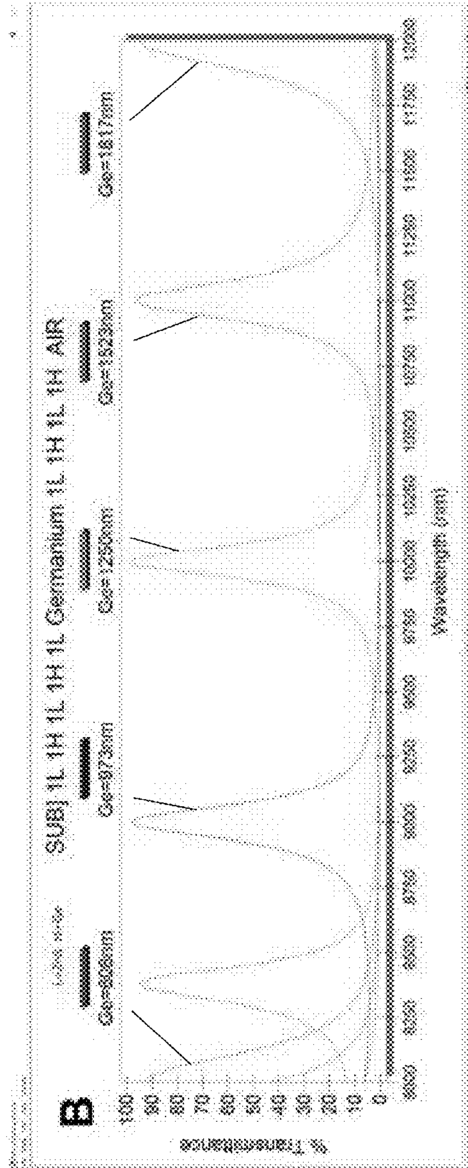

FIG. 6B

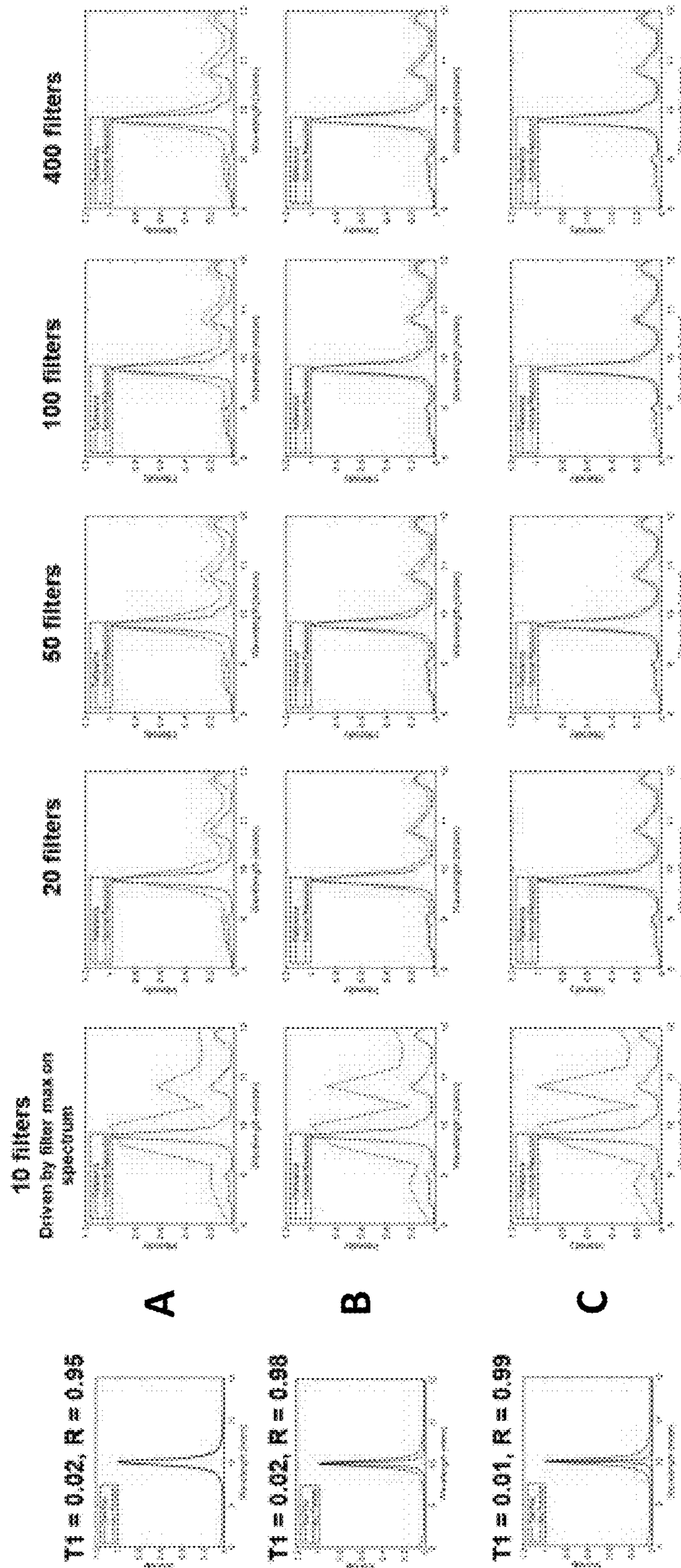

FIG. 7

FIG. 8

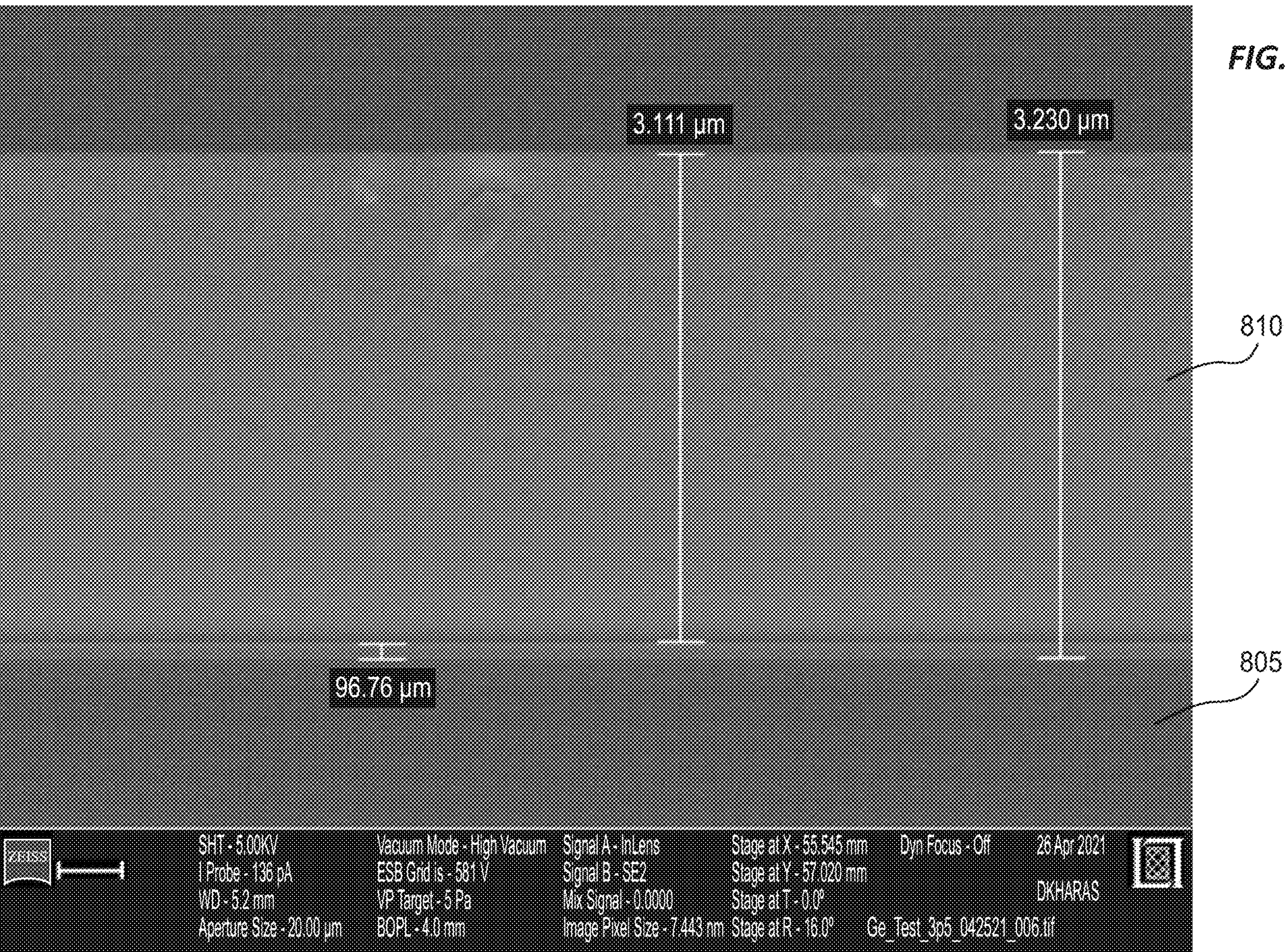

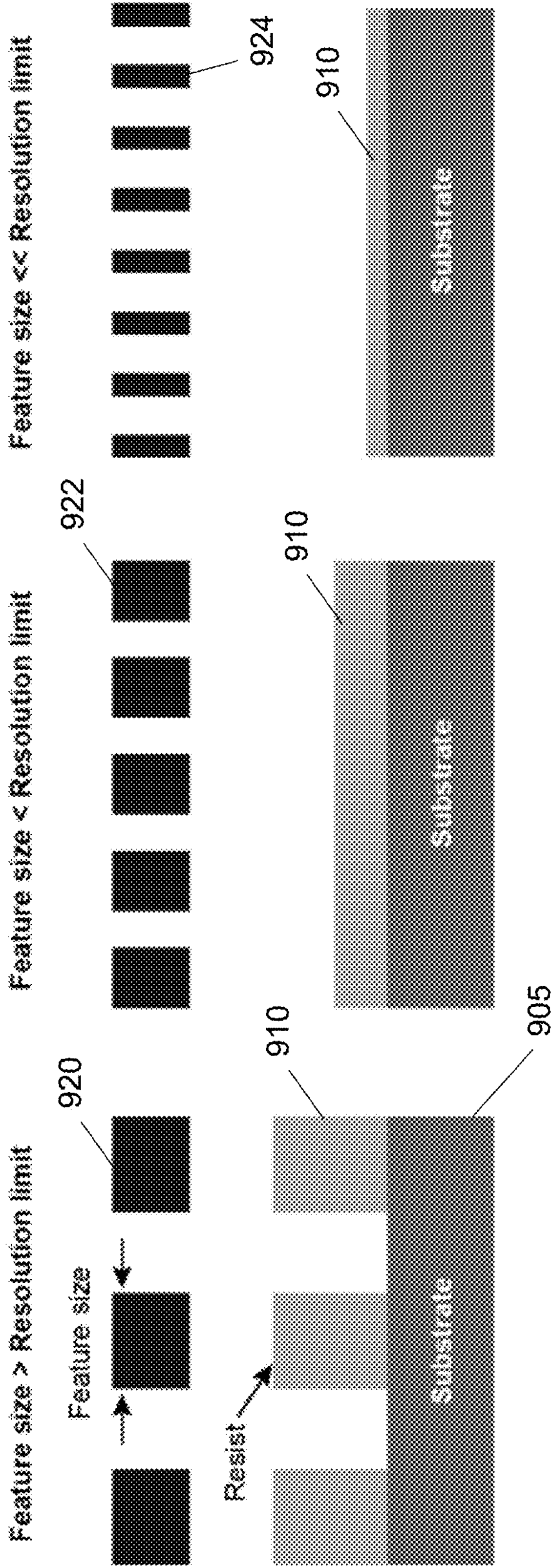

FIG. 9

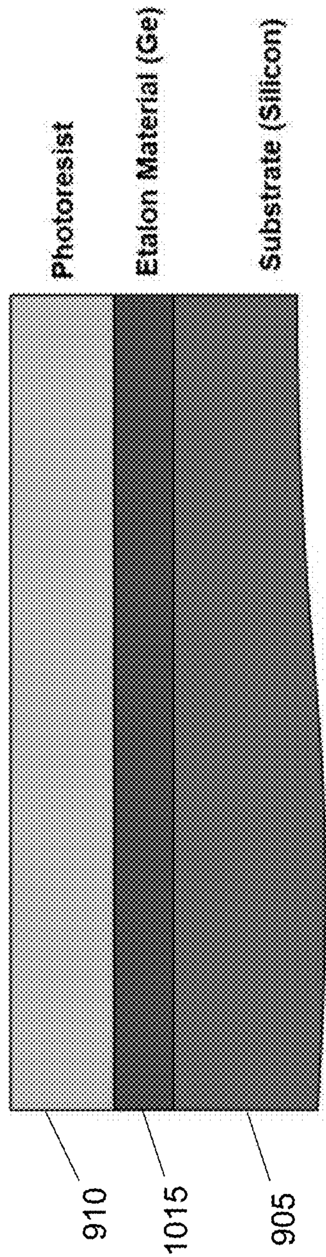

FIG. 10A

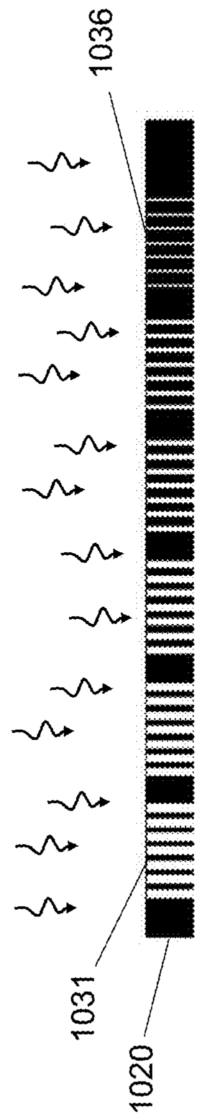

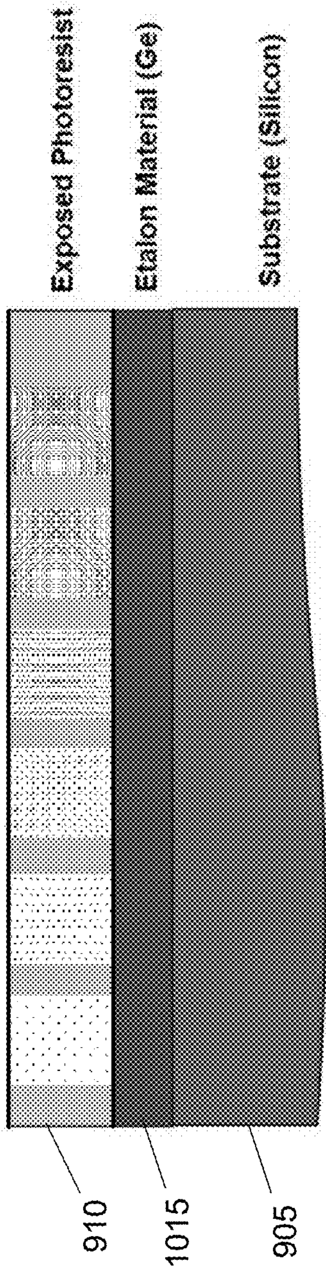

FIG. 10B

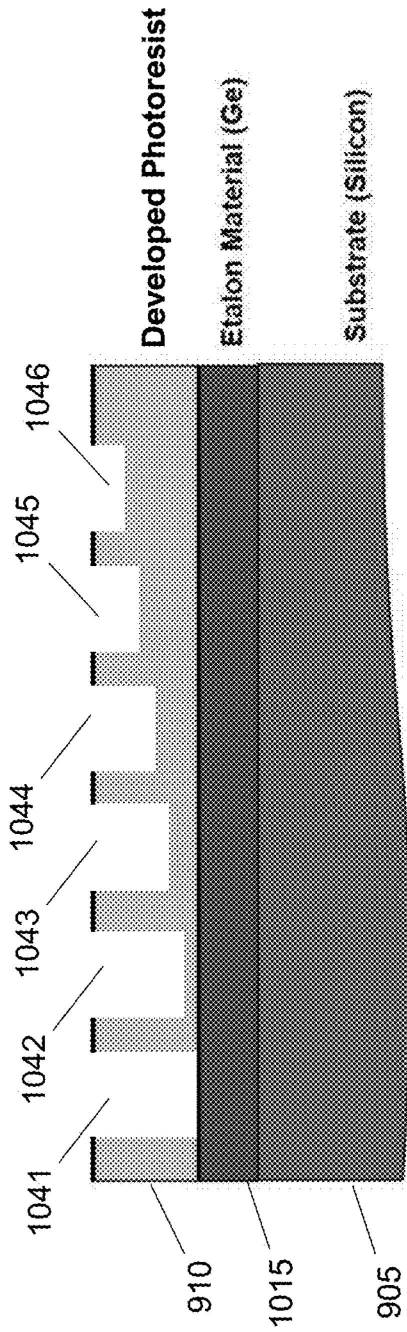

FIG. 10C

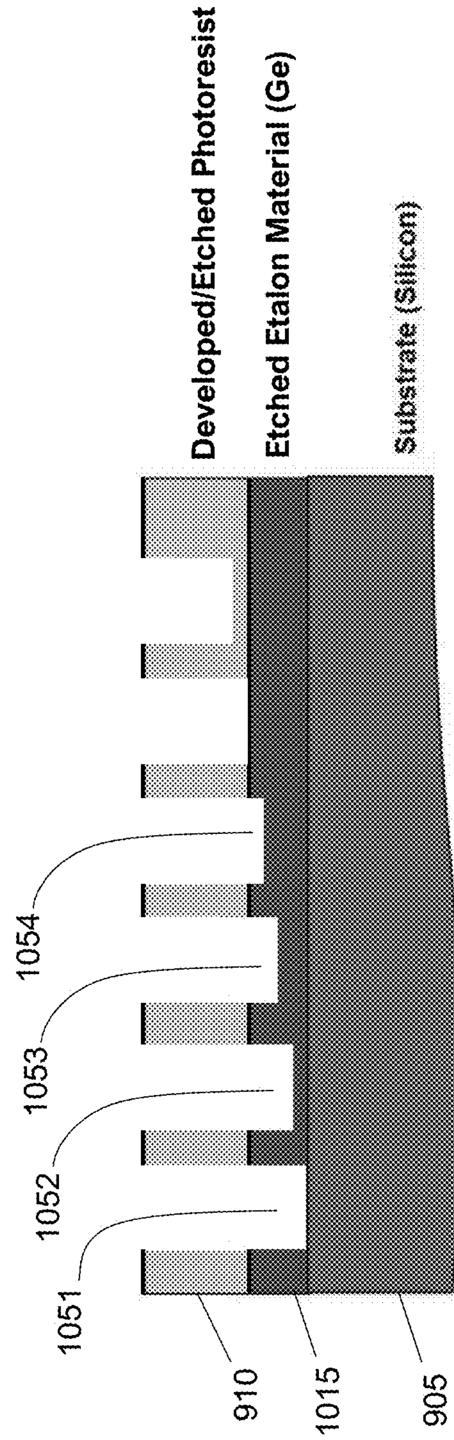

FIG. 10D

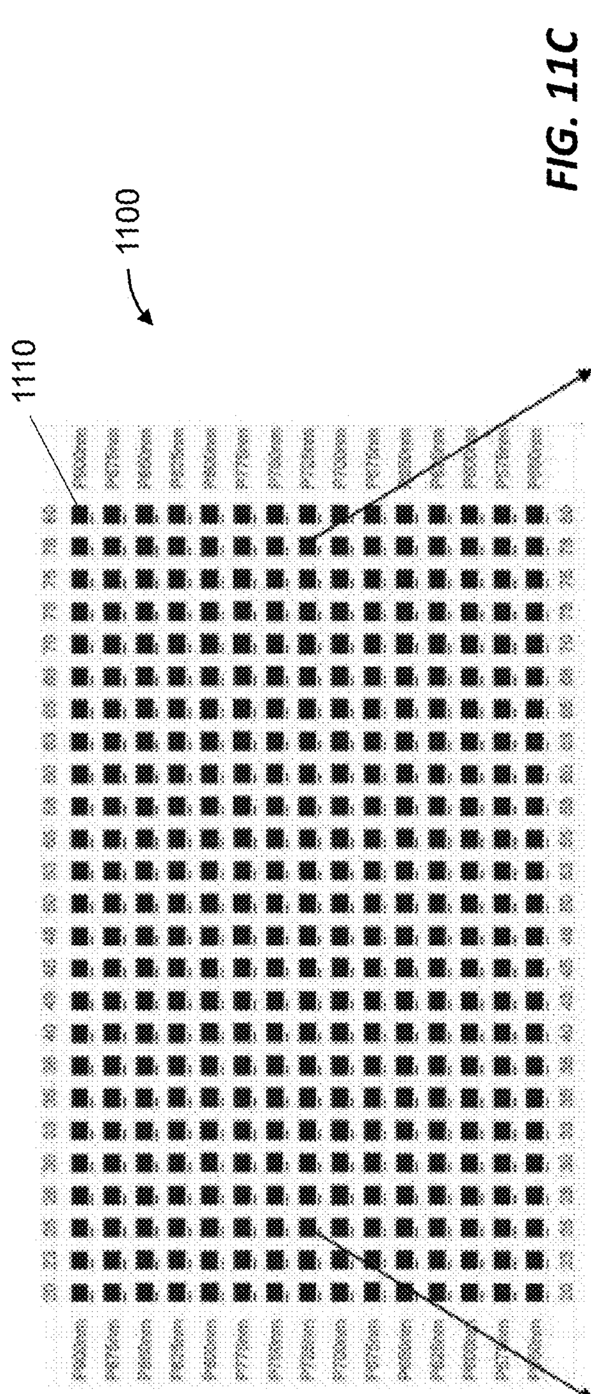

FIG. 11A

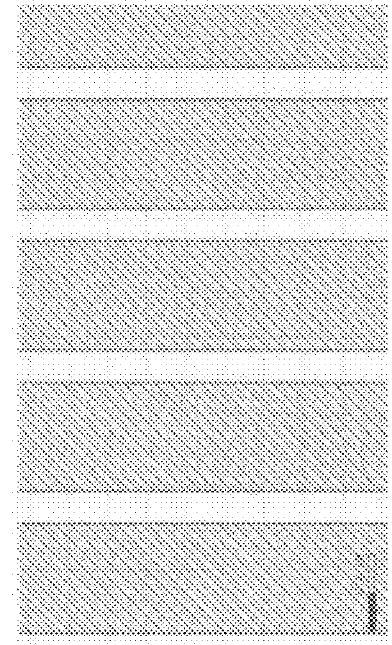

FIG. 11C

P725 LW562 (78%)

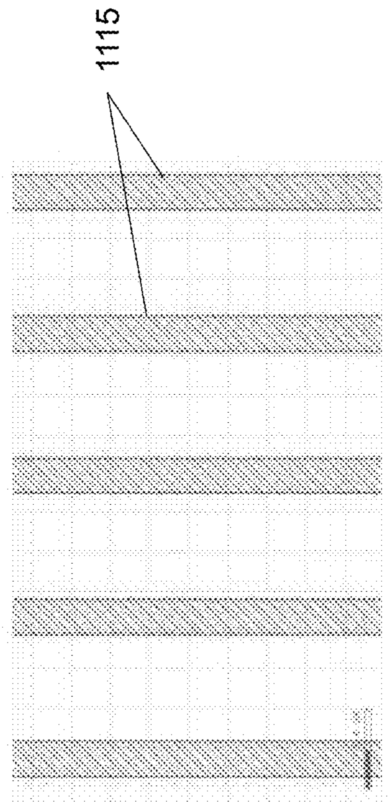

FIG. 11B

P725 LW181 (25%)

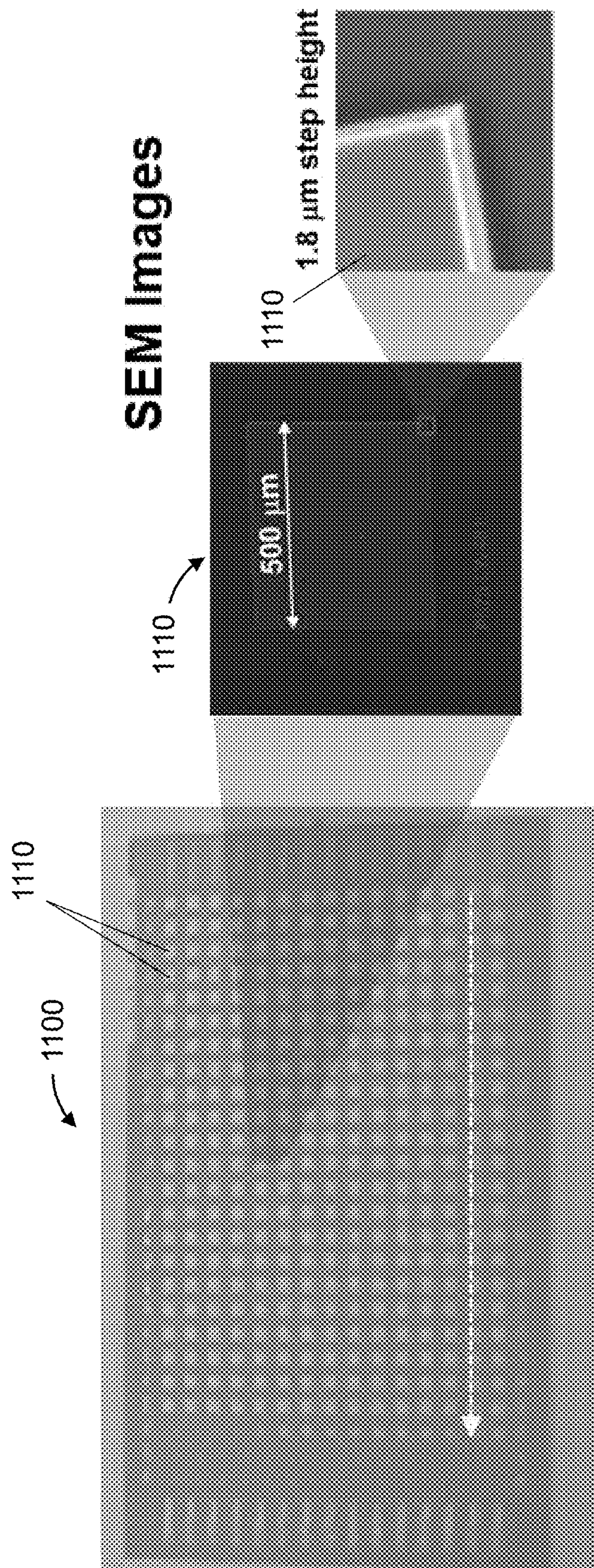

FIG. 12

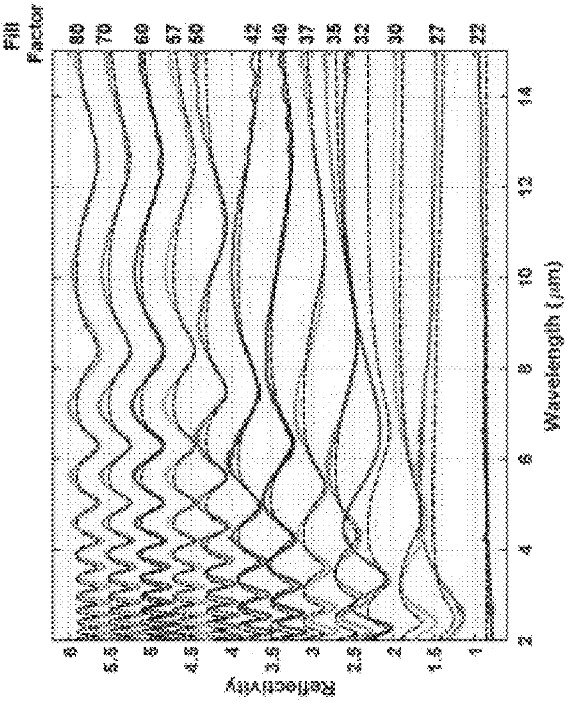

FIG. 14

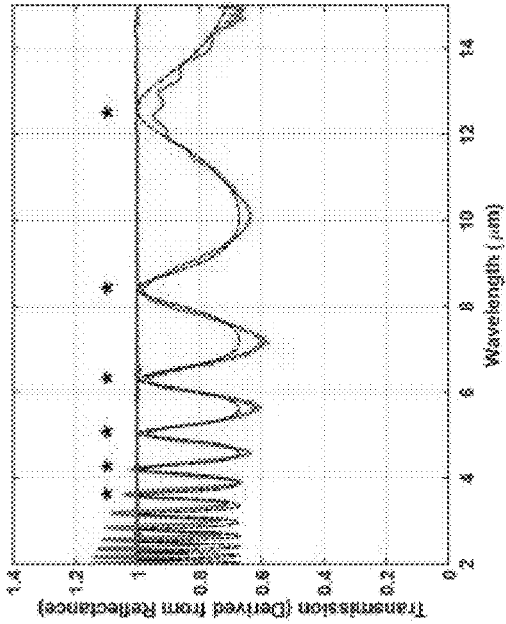

FIG. 13

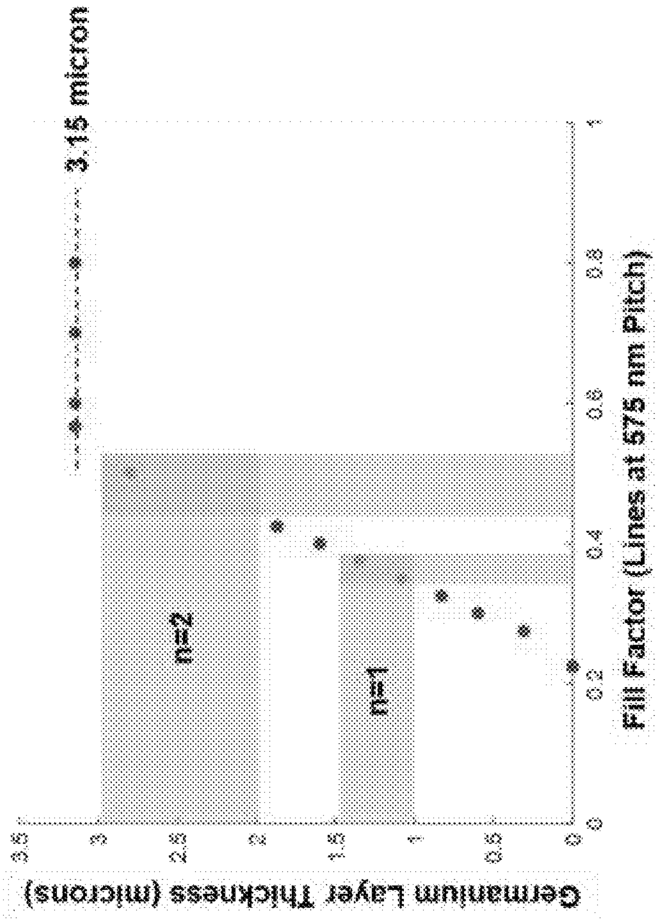

FIG. 15

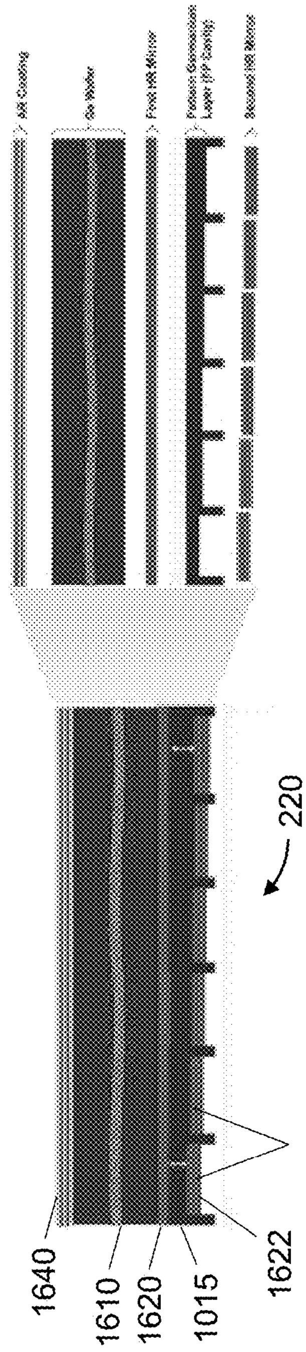

FIG. 16A

FIG. 16B

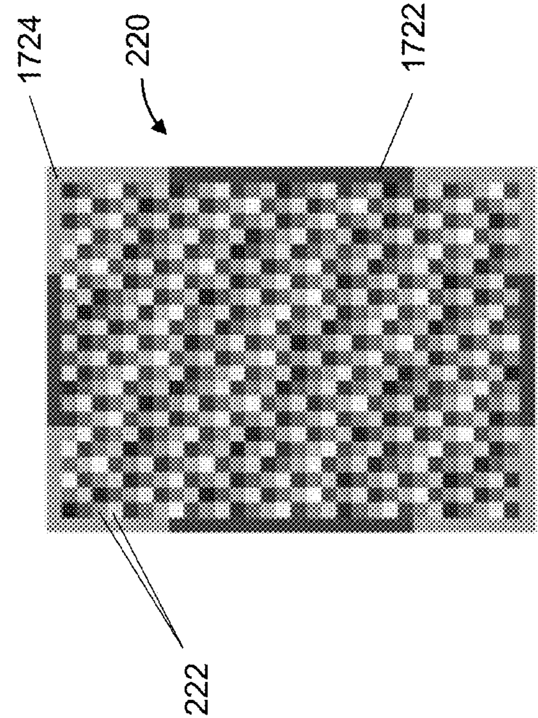

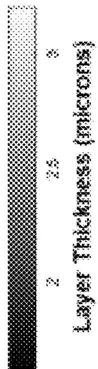

FIG. 17

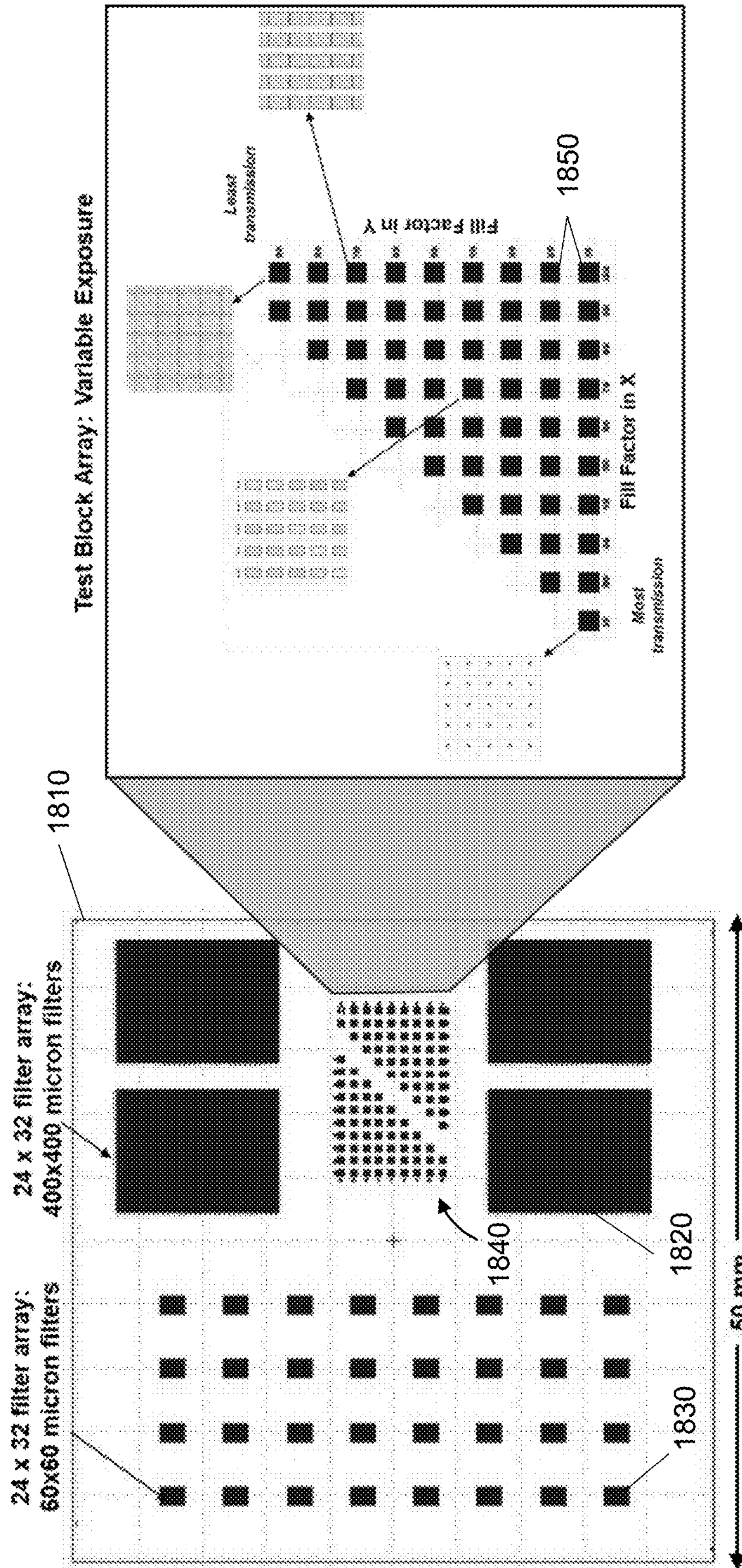

FIG. 18

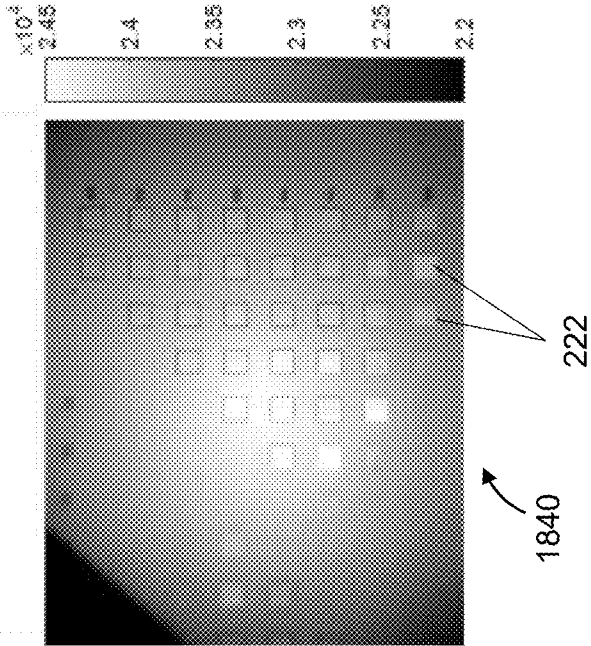

FIG. 19

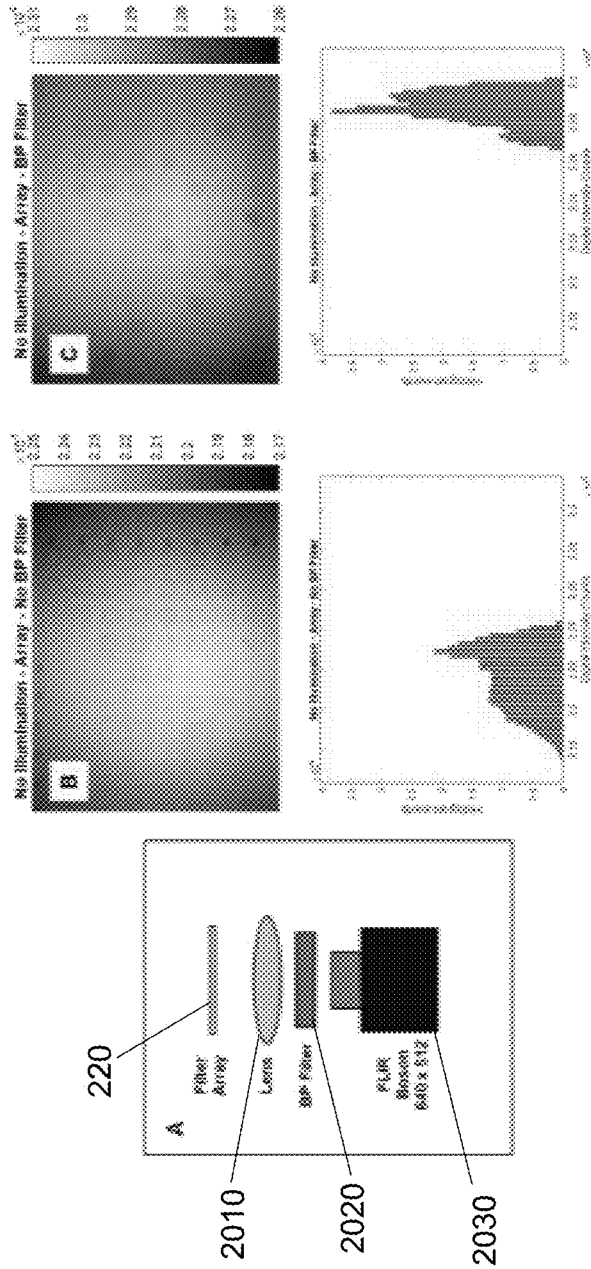

FIG. 20A

FIG. 20B

FIG. 20C

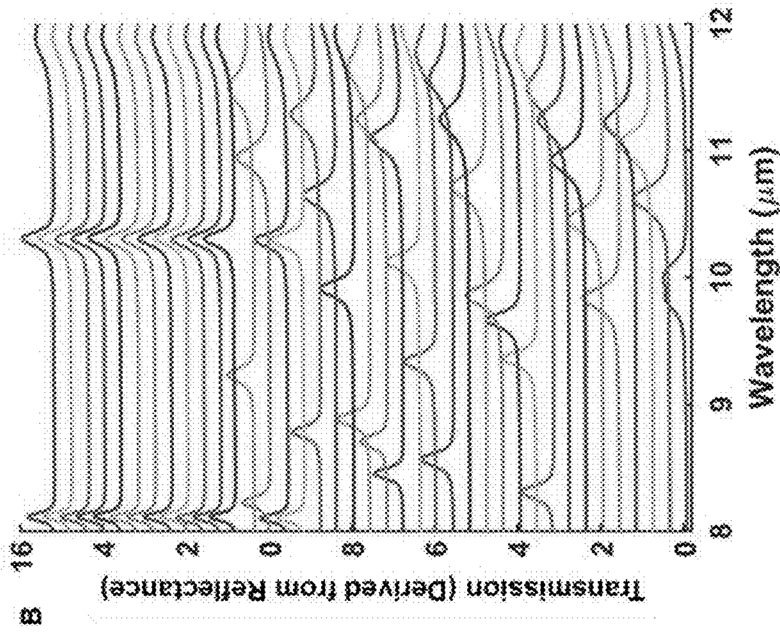

FIG. 21B

A

2030

2010

2020

X- fill factor

Y- fill factor

FIG. 21A

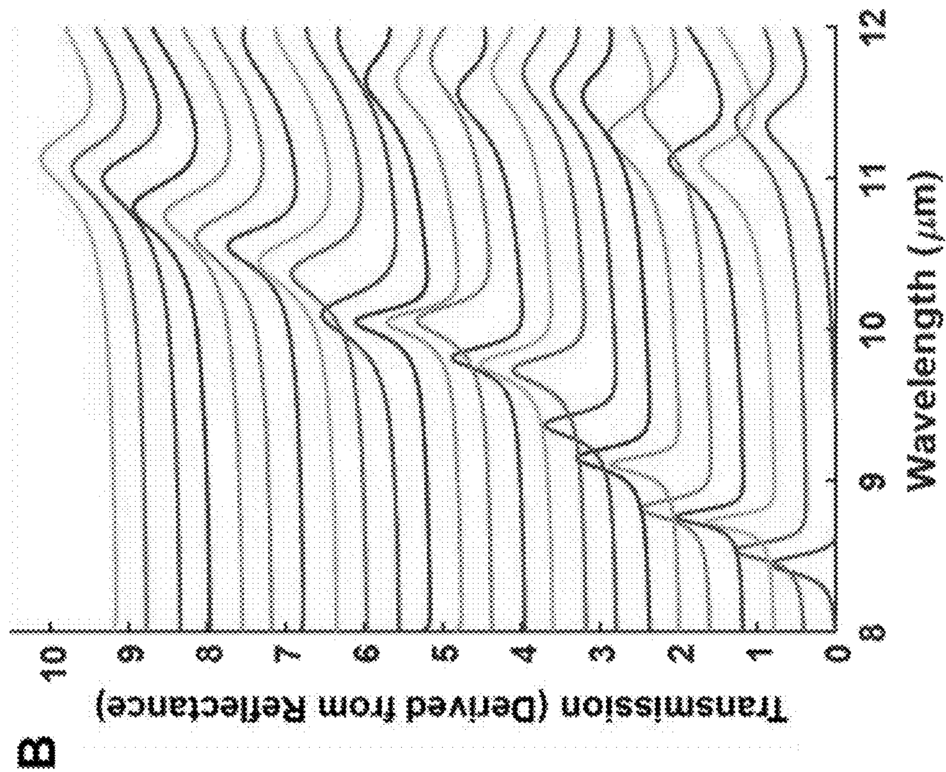

FIG. 22B

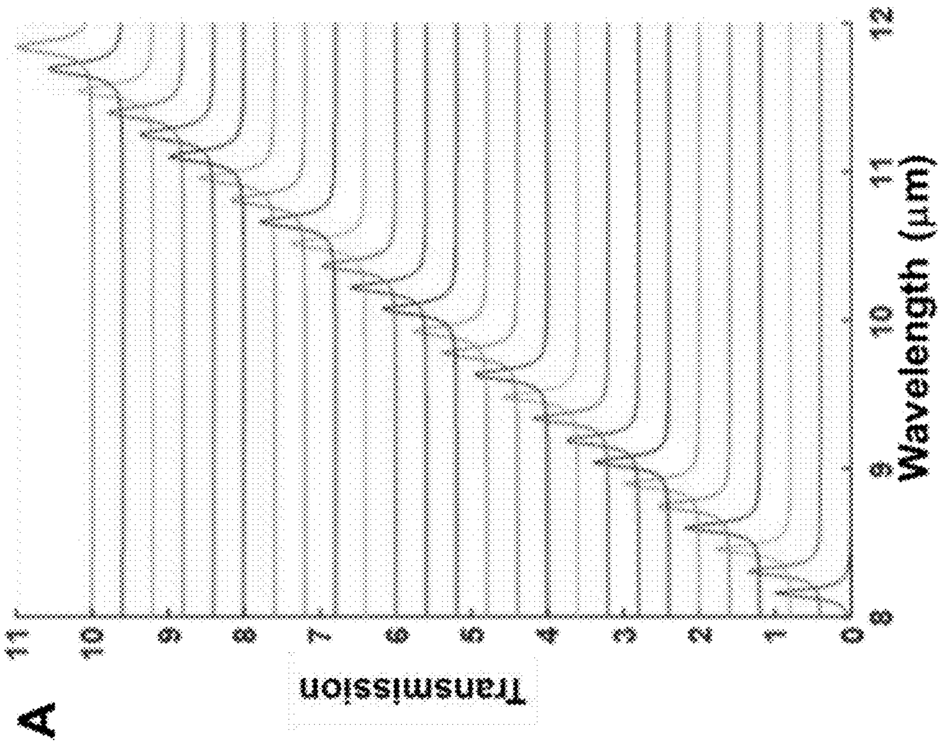

FIG. 22A

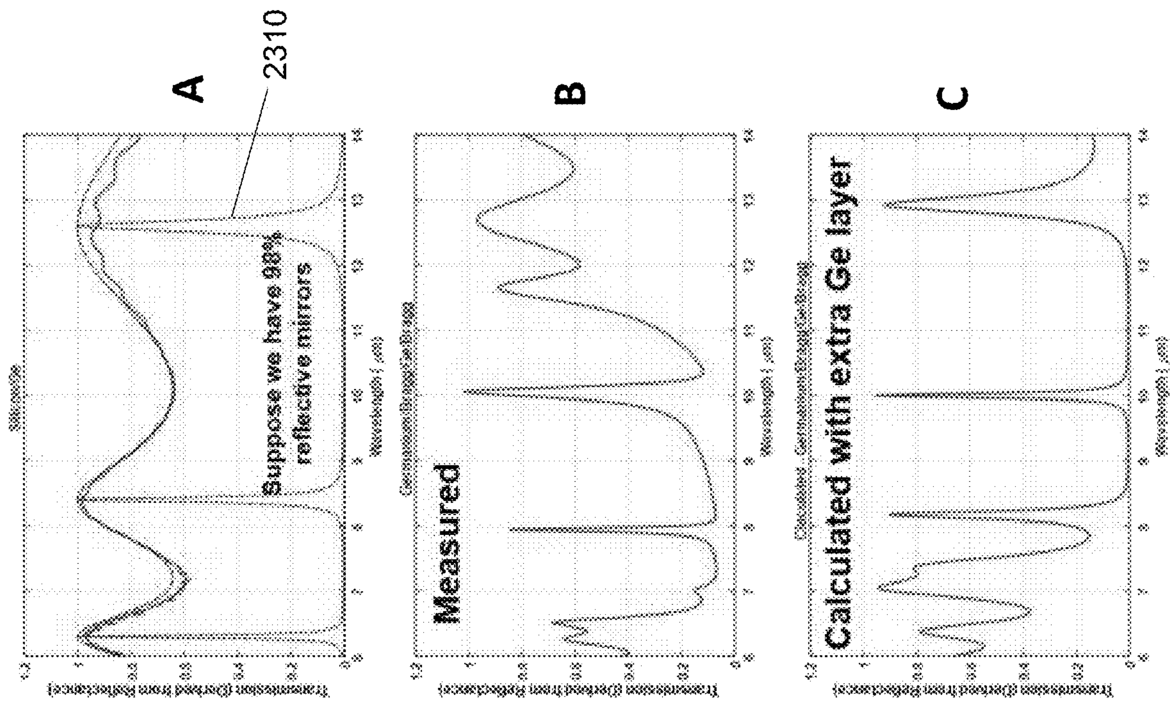

FIG. 23

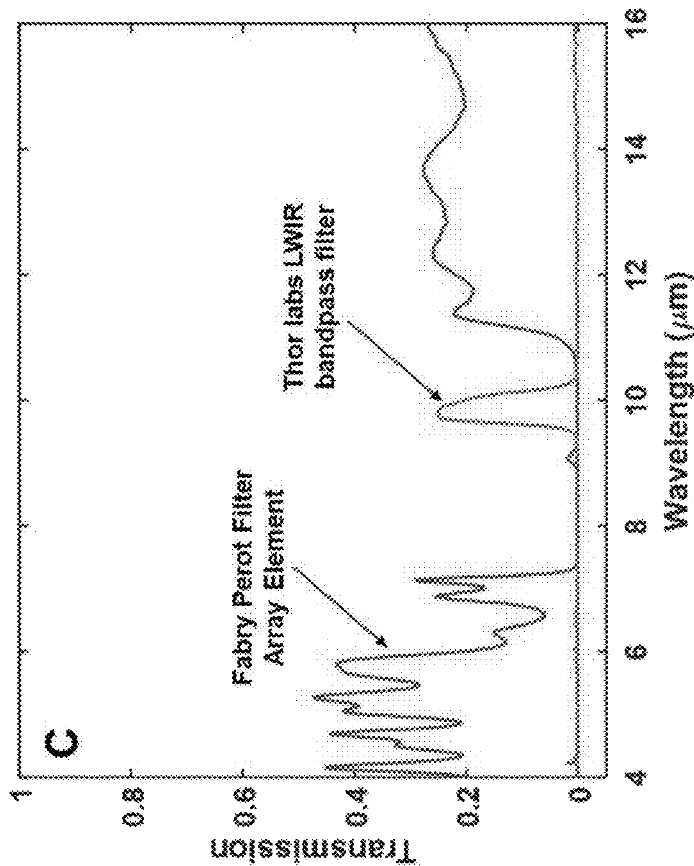

FIG. 24C

FIG. 24A

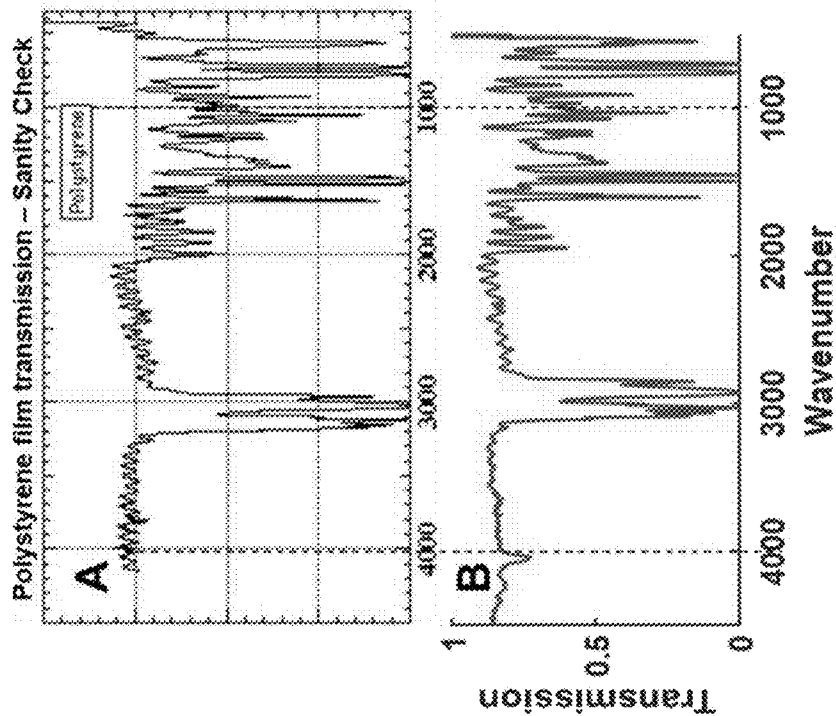

FIG. 24B

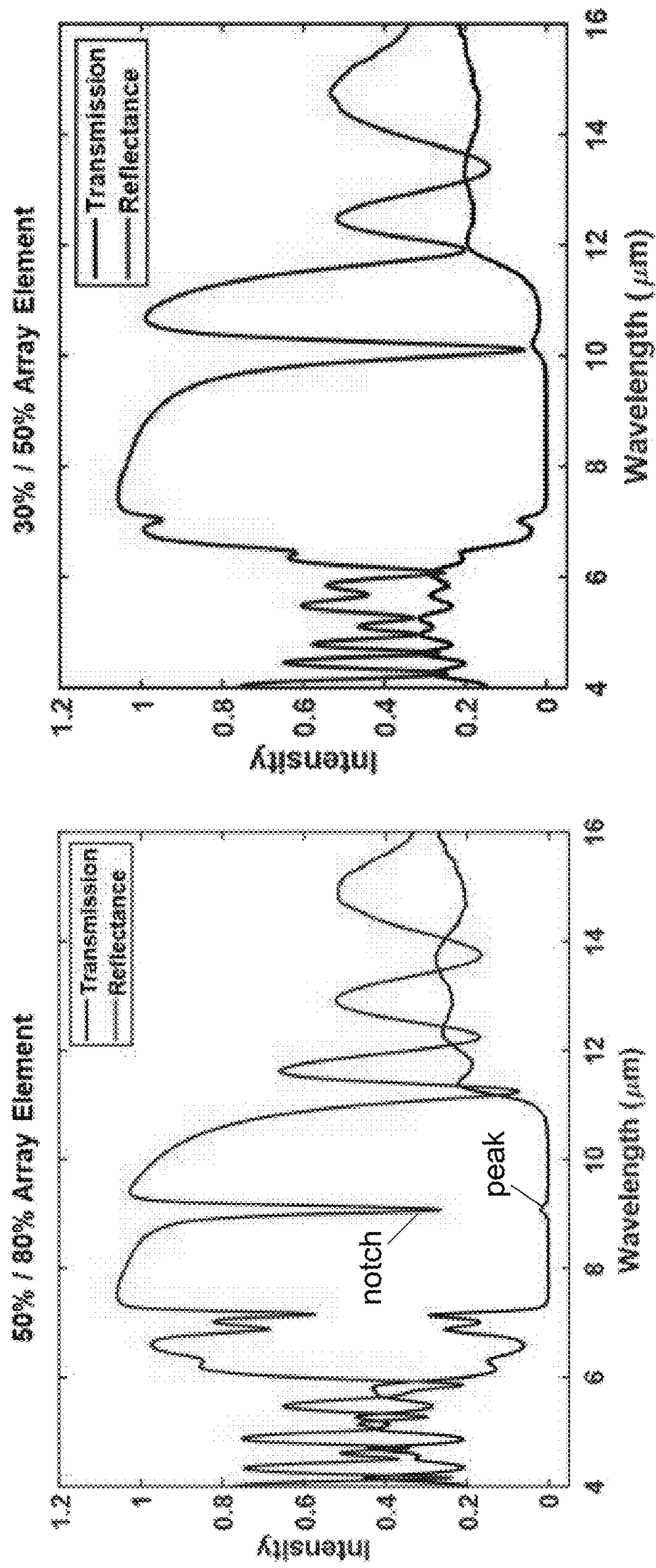

FIG. 25

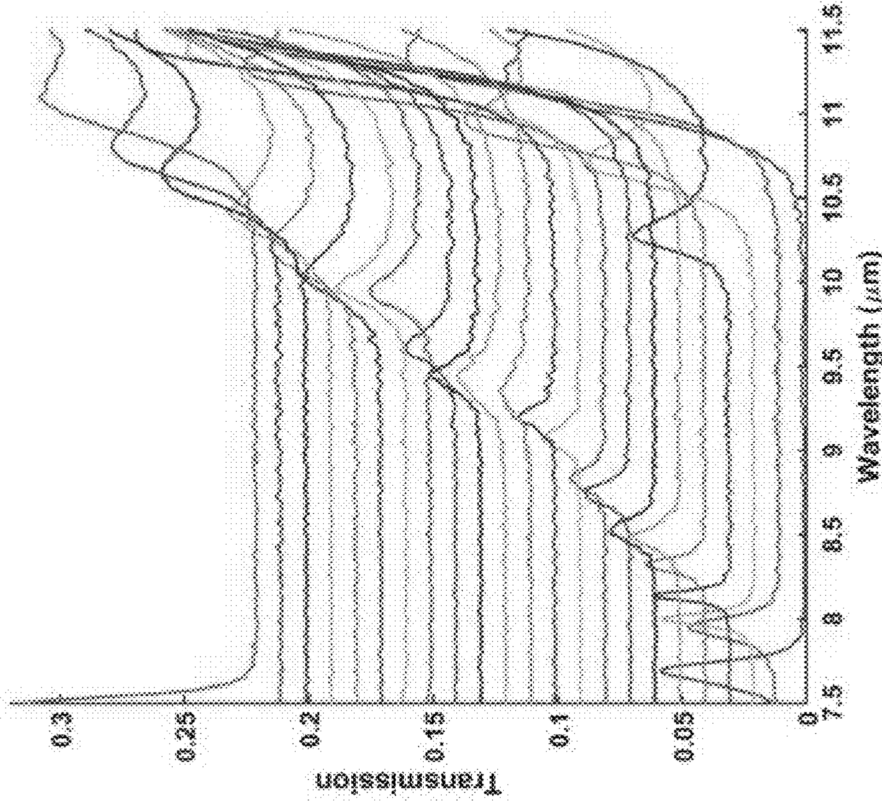

FIG. 26

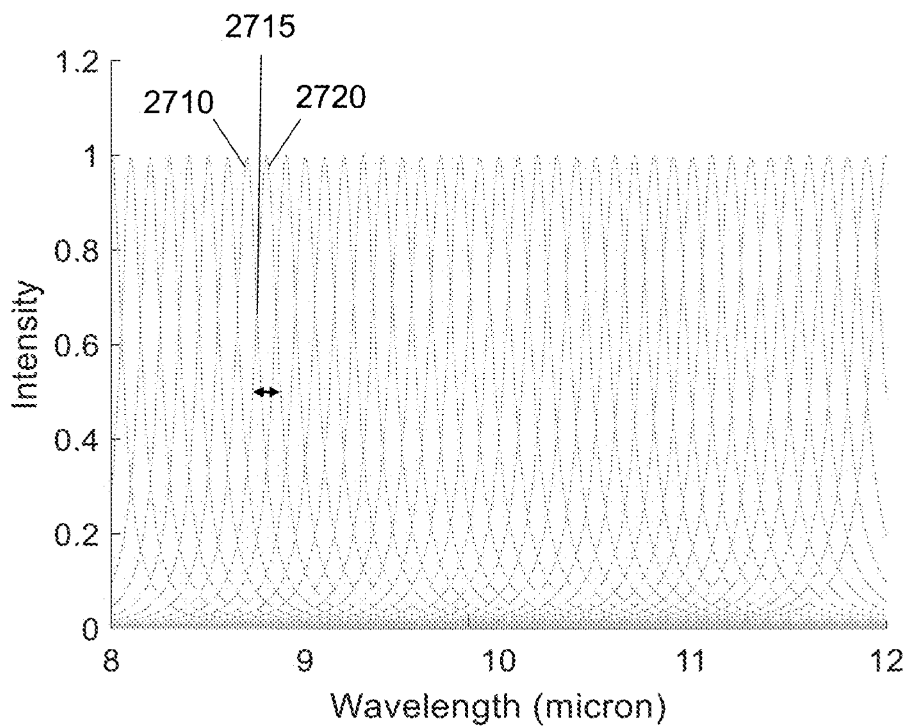

FIG. 27

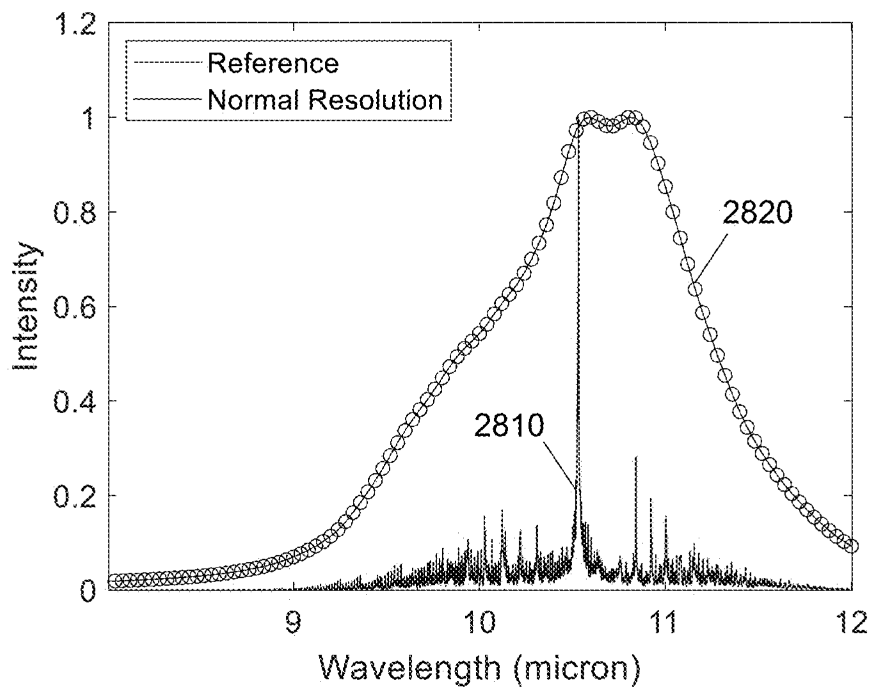

FIG. 28

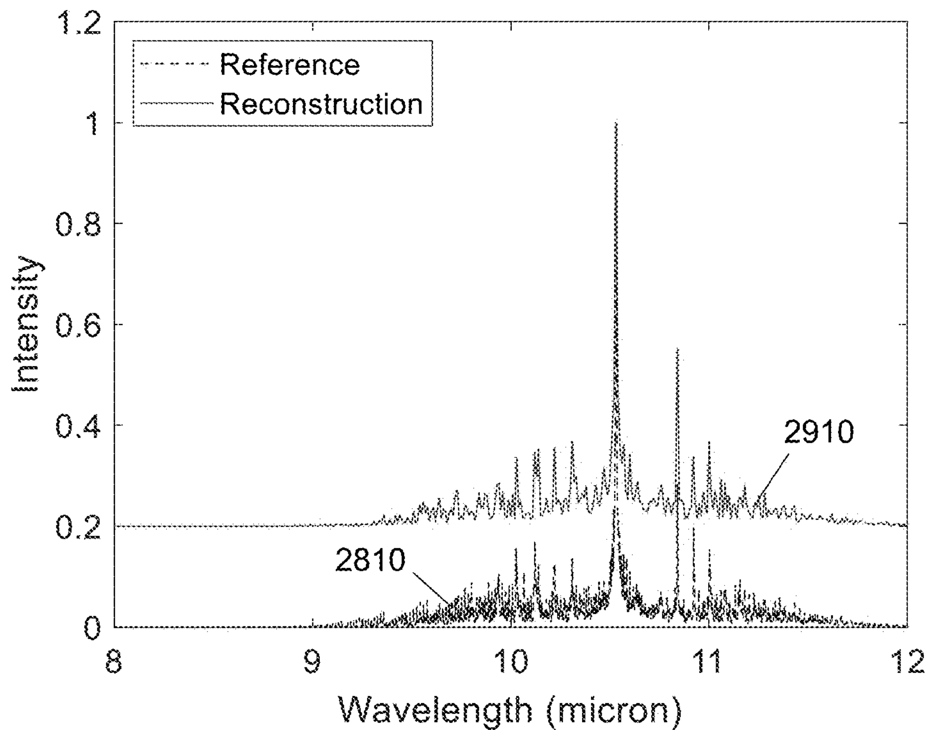

FIG. 29

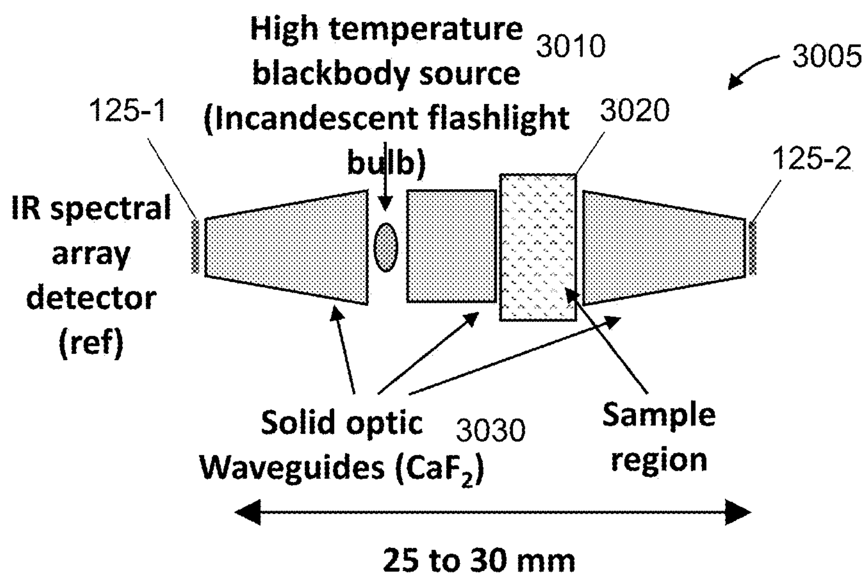

FIG. 30

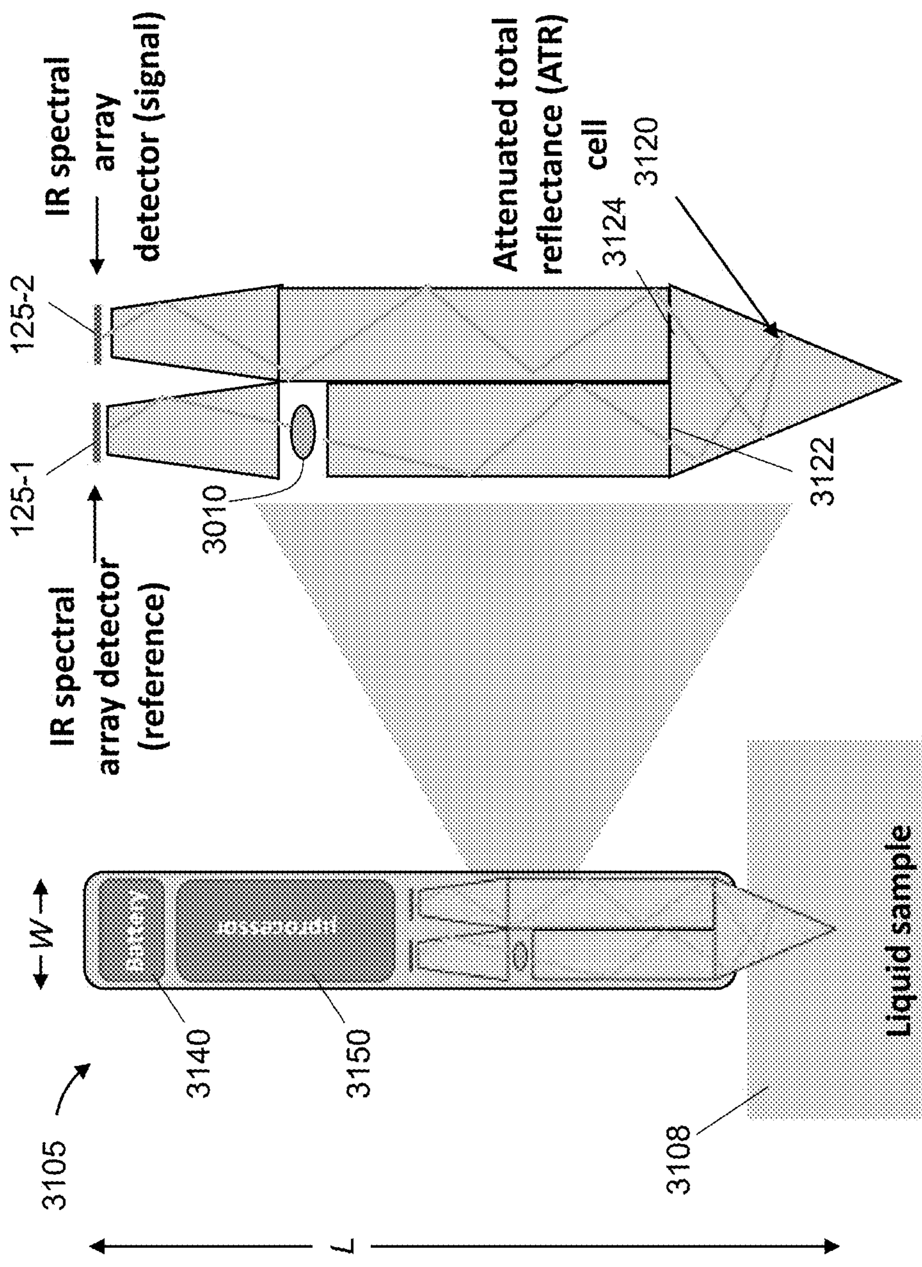

FIG. 31

PIXEL SCALE FABRY PEROT FILTER ARRAY FOR CHEMICAL AGENT VAPOR DETECTION

CROSS-REFERENCE TO RELATED APPLICATION(S)

[0001] This application claims the priority benefit, under 35 U.S.C. 119(e), of U.S. Application No. 63/324,561 titled, "Pixel Scale Fabry-Pérot Filters for Hyperspectral Standoff Chemical Agent Detection," filed Mar. 28, 2022, which is incorporated by reference herein in its entirety for all purposes.

GOVERNMENT SUPPORT

[0002] This invention was made with government support under FA8702-15-D-0001 awarded by the U.S. Air Force. The government has certain rights in the invention.

BACKGROUND

[0003] Passive long wave infrared (LWIR) standoff sensing of chemical warfare agents (CWAs) is a desired capability for the chemical defense infrastructure of the U.S. military. This sensing technique uses the infrared absorption signatures of chemical warfare agents over the 8-micron to 12-micron spectral range to identify threat plumes. Several standoff detection systems are based on Fourier transform infrared (FTIR) spectrometers. In one example standoff detection system, the field-of-view of a single Peltier cooled LWIR detector passes through a Michelson interferometer and scans over the field of regard.

[0004] The application space for these instruments is limited by the size, weight, and power (SWAP) of the instruments. Some of these systems weigh 56-85 pounds and cost hundreds of thousands of dollars. The SWAP requirements limit the use of the sensor to fixed sites or deployment on large mobile platforms, such as trucks or combat vehicles.

SUMMARY

[0005] The present disclosure describes a low-SWAP, low-cost, standoff chip-based spectral sensor that can be used for an integrated, compact spectrometer. The sensor is designed to detect trace gasses or other chemicals in the field-of-view of the sensor or in liquid sampled by the sensor. The sensor is created by directly coupling an array of fixed-frequency Fabry-Pérot filters to a long-wave infrared (LWIR) detector array where different elements of the filter array are tuned to pass different wavelength bands to corresponding detector or detectors in the detector array. The sensor can obtain a spectrally-resolved snapshot of emissions incident on the Fabry-Pérot filters that come from a field-of-view of the sensor. The spectrally-resolved snapshot of the field-of-view can be obtained instantaneously (e.g., in a single data acquisition step of the detector array).

[0006] Some implementations relate to a spectral sensor comprising a first substrate and an array of optical filters formed on the first substrate. Each optical filter can have a first mirror formed on the first substrate, a second mirror spaced apart from the first mirror and in optical communication with the first mirror, and an etalon formed between the first mirror and the second mirror. The spectral sensor can further include a second substrate and an array of detectors formed on the second substrate. The array of detectors can be in optical communication with the array of optical filters. Further, the array of optical filters includes at least 10 optical filters for which the etalons of the 10 optical filters have different thicknesses such that the 10 optical filters have different transmission functions or different reflectivity functions. The etalons of the 10 optical filters having the different thicknesses can all be etched from a same layer of material on the first substrate.

[0007] Some implementations relate to a method of making a spectral sensor. The method can include acts of illuminating a grayscale photomask to expose a photoresist and pattern an array of etalons for Fabry-Pérot filters, wherein the photoresist is deposited over an etalon layer on a substrate; developing the photoresist such that the photoresist has at least 10 different thicknesses over the etalon layer; and etching the photoresist and at least a portion of the etalon layer to pattern the array of etalons, wherein the array of etalons includes at least 10 etalons having different thicknesses.

[0008] All combinations of the foregoing concepts and additional concepts discussed in greater detail below (provided such concepts are not mutually inconsistent) are part of the inventive subject matter disclosed herein. In particular, all combinations of subject matter appearing in this disclosure are part of the inventive subject matter disclosed herein. The terminology used herein that also may appear in any disclosure incorporated by reference should be accorded a meaning most consistent with the particular concepts disclosed herein.

BRIEF DESCRIPTIONS OF THE DRAWINGS

[0009] The skilled artisan will understand that the drawings primarily are for illustrative purposes and are not intended to limit the scope of the inventive subject matter described herein. The drawings are not necessarily to scale; in some instances, various aspects of the inventive subject matter disclosed herein may be shown exaggerated or enlarged in the drawings to facilitate an understanding of different features. In the drawings, like reference characters generally refer to like features (e.g., functionally and/or structurally similar elements).

[0010] FIG. **1** illustrates an example application for a hyperspectral standoff snapshot spectral sensor deployed on a micro-unmanned aerial vehicle for chemical warfare agent detection.

[0011] FIG. **2** depicts components of a spectral sensor and a packaged spectrometer.

[0012] FIG. **3** illustrates the components and packaged spectrometer of FIG. **2** along with target transmission functions or bandpasses for the filters in the Fabry-Pérot filter array.

[0013] FIG. **4** illustrates operation of the Fabry-Pérot filters. The optical bandpass of the filter depends on the optical path length between the mirror surfaces.

[0014] FIG. **5** is a plot of transmission as a function of wavelength from EQ. 1 for different mirror reflectivities, a 5-micron mirror separation, and cavity refractive index of 1.

[0015] FIG. **6**A and FIG. **6**B are plots of filter performance as a function of the number of layers for a 1-pair Bragg mirror (A) and a 2-pair Bragg mirror (B).

[0016] FIG. **7** illustrates spectrum measurement fidelity based on the filter bandwidth and the number of different filter frequencies in the Fabry-Pérot filter array. The spectrum of Sarin CWA is used as a test case.

[0017] FIG. **8** shows a scanning electron microscope image of a cross-section of a germanium layer on a silicon wafer.

[0018] FIG. **9** illustrates the impact of feature size in the photomask and the resist profile as a function of the ratio of feature size to resolution limit. From Smith et al., J. Micro/Nano MEMS MOEMS 18(4) 043507 (2019), which is incorporated herein by reference in its entirety.

[0019] FIG. **10**A, FIG. **10**B, FIG. **10**C, and FIG. **10**D depict structures formed in a grayscale photolithography process.

[0020] FIG. **11**A, FIG. **11**B, and FIG. **11**C show the mask layout of a grayscale photolithography mask. FIG. **11**A: Test block from the mask which is a matrix of pitch (along vertical axis) and fill factor (along the horizontal axis). FIG. **11**B and FIG. **11**C are detail examples of different fill factors at the same pitch.

[0021] FIG. **12** shows a visible image (left) of the etched germanium features on the silicon wafer using the test block in the mask of FIG. **11**A. Scanning electron microscope (SEM) images (right) show the step height and uniform top surface of the germanium features.

[0022] FIG. **13** is a plot of calculated transmission (obtained by subtracting the measured reflectance from 1) for a germanium etalon produced from a 575-nm-pitch, 480-nm-line-space grayscale mask. The "transmission" maxima are marked with asterisks and the dashed line is the fit of the data using EQ. 1 with 0.11 for mirror reflectivity and 3.15-micron thick germanium.

[0023] FIG. **14** is a plot of measured reflectance of germanium features from the test matrix at different fill factors (as indicated on the right of the graph). Spectra are offset vertically for clarity.

[0024] FIG. **15** is a plot of the thickness measurement of germanium feature based on FTIR reflectance measurements in FIG. **14**. The shaded areas indicate the working range for the LWIR germanium layer thickness for first- and second-order Fabry-Pérot transmission peaks.

[0025] FIG. **16**A and FIG. **16**B show a Fabry-Pérot Filter array (A) and an exploded view (B) of the components of the Fabry-Pérot filter array (not to scale).

[0026] FIG. **17** shows a layout of the mask that will define the cavity thickness in the Fabry-Pérot filter. There are 132 gray scale values. Each value is repeated 5 times in a pseudo random spatial pattern across the array.

[0027] FIG. **18** shows a die layout for the 50×50 mm exposure field of a Canon i-line stepper.

[0028] FIG. **19** is an image of a test block array (produced from the die and mask of FIG. **18**) recorded using the FUR Boson camera with a Globar blackbody source behind the filter array.

[0029] FIG. **20**A shows optics for recording images with a FLTR Boson camera.

[0030] FIG. **20**B shows an image (top) and histogram (bottom) of the array of FIG. **19** with no bandpass filter.

[0031] FIG. **20**C shows an image (top) and histogram (bottom) of the array of FIG. **19** with the bandpass filter.

[0032] FIG. **21**A and FIG. **21**B illustrate the dependence of filter spectrum as a function of relative exposure intensity. FIG. **21**A: Matrix of relative exposure intensity as a function of x and y fill factor. Shading on the bottom rows indicates overexposure and no remaining germanium, shading on the middle rows indicates within the exposure window with variation in germanium step height, and shading in the upper rows indicates underexposure with no change in germanium step height. FIG. **21**B: Spectra of the upper- and middle-row filter locations—all of the filters in the upper rows have similar spectra.

[0033] FIG. **22**A and FIG. **22**B illustrate objective versus measured filer performance. FIG. **22**A: objective (idealized) filter performance depicted in FIG. **3**. FIG. **22**B: Measured reflectance cast as transmission (transmission=1−reflectance) for the filter test block.

[0034] FIG. **23** shows reflectance measurements cast as transmission for different system.

[0035] FIG. **24**A, FIG. **24**B, and FIG. **24**C illustrate initial transmission measurements using the FTIR microscope. FIG. **24**A: Literature spectrum of a polystyrene film. FIG. **24**B: Measured spectrum of polystyrene film. FIG. **24**C: Transmission measurement of a Fabry-Pérot filter element and the Thor Labs bandpass filter (10-micron center wavelength−0.5-micron full width half maximum).

[0036] FIG. **25** shows a comparison of reflectance and transmission measurements for two different elements in the test block.

[0037] FIG. **26** shows the measured transmission of the test block filter array.

[0038] FIG. **27** plots overlapping transmission functions for an array of Fabry-Pérot filters.

[0039] FIG. **28** plots a reference spectrum and a measured spectrum using a Fabry-Pérot filter array with overlapping transmission functions.

[0040] FIG. **29** plots a deconvolved spectrum obtained from the measured spectrum of FIG. **28** and plots the reference spectrum for comparison.

[0041] FIG. **30** depicts an example of a compact spectrometer for spectral analysis of a sample.

[0042] FIG. **31** depicts another example of a compact spectrometer for spectral analysis of a liquid sample.

DETAILED DESCRIPTION

1. Overview

[0043] An example application for a standoff spectral sensor **125** with low-SWAP characteristics is illustrated in FIG. **1**. In some cases, the standoff spectral sensor **125** is compatible with operation of a lightweight, unmanned aerial vehicle (UAV) **120** (e.g., a UAV **120** that weighs less than 20 pounds and has an operating altitude less than 1,200 feet above ground level). The spectral sensor **125** can detect, identify, and map vapor phase chemical warfare agent threats in a field forward operation **100**. Multiple UAVs **120** with the standoff chemical agent sensors **125** can be used to monitor a large area in such an operation. Each UAV **120** can act independently to monitor a defined area of regard. If a UAV **120** detects a threat plume **140** it would signal to other UAVs **120** to move to the area of detection and the UAVs **120** would begin to cooperatively map and track the release plume **140**.

[0044] The standoff spectral sensor **125** can have significantly reduced size, weight, and power limitations as well as reduced cost compared to conventional chemical sensors. The spectral sensor **125** is compact and lightweight such that it could be mounted on UAVs **120** described above. An example of the spectral sensor **125** is depicted in FIG. **2**. The standoff spectral sensor **125** can be chip-scale and integrated into a spectrometer. The spectral sensor **125** comprises a detector array **210** of LWIR detectors **212** and a filter array

220 of fixed bandwidth Fabry-Pérot filters 222 (having different spectral passbands) optically coupled to pixels of the detector array. In some implementations, the spectral sensor 125 can be packaged with additional optics and other spectrometer components (e.g., power source, controller, memory, etc.) in a housing, such as a packaged spectral camera 240.

[0045] Each Fabry-Pérot filter 222 in the filter array 220 passes a narrow optical wavelength band to one or more corresponding detectors 212 in the detector array 210. Multiple Fabry-Pérot filters 222 can be tuned to pass (or reflect for a reflection implementation) different wavelength bands. As an example, a 160×120 LWIR detector array 210 (such as the low cost, low-SWAP FLIR Lepton 3) has a total of 19,200 detectors 212. The filter array 220 can be composed of 32×24 filter elements where each Fabry-Pérot filter 222 covers a 5×5 set of detectors 212. If each Fabry-Pérot filter 222 was a different wavelength band, the 32×24 element array could detect as many as 768 different wavelength bands. Each wavelength band can be a narrow range of wavelengths (e.g., a full-width-half-maximum (FWHM) bandwidth between 10 nm and 1000 nm for center wavelengths in a range from 8 microns to 12 microns). In some implementations, a wavelength band can have a FWHM bandwidth between 250 nm and 750 nm.

[0046] The inventor has determined that it is not practical or necessary to have 768 different wavelength bands for a low-SWAP spectral sensor 125 that operates in the range of interest (8 microns to 12 microns). Instead, the spectral sensor 125 can be fabricated to detect 132 different wavelength bands with 40 nm spectral spacing and each wavelength band is reproduced 5 times. This filter layout can provide IR spectral coverage from 7.36 microns to 12.64 microns. For some applications, even fewer wavelength bands (e.g., no more than 20 or no more than 40) can be used for adequate spectral coverage.

[0047] Such an example standoff spectral sensor 125 can provide functionality that is not currently available. A Peltier-cooled version of this standoff sensor provides a standoff range of up to 5 km and even up to 10 km and sensitivity of other, heavier, more complicated devices. For example, a Peltier cooler 250 can be thermally contacted to a spectral sensor 125 that is formed on a substrate 205. Uncooled versions of this standoff spectral sensor 125 provide new operational sensing capability as a result of greatly reduced SWAP and cost. The uncooled standoff spectral sensor 125 may have less range (e.g., up to 1 km) than a cooled version, but the uncooled version could be mounted on UAVs or used as person borne (helmet or suit) systems. These low-SWAP standoff spectral sensors 125 could be used as a swarm of UAVs to monitor a large battlespace and autonomously map CWA threat plumes 140 in three dimensions. Helmet mounted systems could be used by first responders to provide situational awareness as they enter laboratories, factories, warehouses, buildings, or other hazardous situations (e.g., fires where there may be a release of hazardous chemicals).

[0048] An example implementation of the spectral sensor 125 described herein is based on a 32×24 element filter array 220. The outer edge elements, or an outer portion, of the filter array 220 can be used for testing and alignment. The remaining elements in the filter array 220 (30×22 elements in this example) comprise 660 Fabry-Pérot filters 222 which can be divided into 132 different wavelength bands with each wavelength band reproduced five times in the filter array 220. The filter array 220 can provide 0.04-micron wavelength separation between center wavelengths for each wavelength band to cover the 7.36 micron to 12.64 wavelength range. The filter array 220 can be sized to fit different sized detector arrays 210. One implementation of the filter array 220 includes 60-micron-square Fabry-Pérot filters 222. Another implementation includes 400-micron-square Fabry-Pérot filters 222. Each Fabry-Pérot filter 222 can cover multiple detectors 212, though the invention is not so limited. In some implementations, one Fabry-Pérot filter 222 can cover only one detector 212. Each detector 212 can couple to only one Fabry-Pérot filter 222 but each Fabry-Pérot filter 222 can be coupled to one or more detectors 212.

[0049] Gray-scale photolithography can be used, in part, to fabricate the Fabry-Pérot filters 222 that pass or reflect different wavelength bands as described below. At least one optical component 230 included with the spectral sensor 125 (e.g., as part of a packaged spectral camera 240) can be adapted to homogenize emissions from the field-of-view across all of the detector array 210 and eliminate the spatial dependence of the field-of-view in the spectral domain. Homogenizing the emissions can avoid missing detection of a spectral component that occupies a small region in the field of view. For example, its image could fall only on one or more filters that do not pass the wavelength band from that small region. In such an implementation, the packaged spectral camera 240 can be a non-imaging camera. The optical component(s) 230 can include a random phase plate, diffusor, fly's-eye or micro lenses, prismatic sheets, etc. or some combination thereof.

[0050] Example filter arrays 220 can be fabricated using photolithographic and etch methods to form different etch depths (and etalon cavity thicknesses) in a germanium or other semiconductor cavity layer. A grayscale photolithography mask can be used to pattern the Fabry-Pérot filter array 220. The different cavity thicknesses determine the center wavelength of each Fabry-Pérot filter 222. In one example, a fabricated device wafer includes test structures, and 24×32 element Fabry-Pérot filter arrays 220 with 60×60-micron filter elements and 400×400-micron filter elements. The thicknesses of the etalons can be measured using an FTIR microscope. The FTIR microscope can also be used to characterize the optical properties of the Fabry-Pérot filters 222. Reflectance measurements show the fabrication of optical cavities where the cavity thickness, and therefore the transmission wavelength, of the Fabry-Pérot filter 222 was defined by the gray scale lithography.

[0051] Additionally, a 400×400 element filter array 220 is coupled to a FLTR Boson detector array 210 to record scene radiance as a function of temperature. These measurements show the wavelength-dependent filter response as a function of the cavity thickness. Further details are presented in the following sections.

2. Fabry-Pérot Filter Array

[0052] FIG. 3 illustrates the operation of an example hyperspectral standoff spectral sensor 125 (which may also be referred to as a "snapshot sensor") that includes a Fabry-Pérot filter array 220. The Fabry-Pérot filter array 220 is in optical communication with a detector array 210 of the spectral sensor 125. Camera optics 310 (which can include optical components 230 of FIG. 2) are designed to evenly illuminate the filter array 220 with the radiance from the

camera's field-of-view. Radiance from the scene viewed by the camera **240** is incident on the Fabry-Pérot filters **222** and each filter has a defined bandpass as depicted by the multiple wavelength plots **320** in FIG. **3**. There are 26 different bandpasses plotted in FIG. **3**. Radiance in a filter's passband is transmitted to one or more corresponding detectors **212** in one or more pixels of the detector array **210** behind the filter array **220**. Depending on the design of the filter array **220** and the detector array **210**, from 1 to 100 detectors can be illuminated with radiation passed by a single Fabry-Pérot filter **222**, though a larger number of detectors may be illuminated by a single filter in some applications.

[0053] The intensity signals from the detectors **212** behind the corresponding Fabry-Pérot filter **222** can be averaged to provide the scene radiance for the wavelength band passed by that Fabry-Pérot filter **222** to the corresponding detector (s) **212**. The average intensity is used to produce one point on the radiance spectrum **330**, also plotted in FIG. **3**. If the Fabry-Pérot bandpass is repeated with other filters **222** in the filter array **220**, the average intensity values from each repeated filter can be averaged together to produce a point on the radiance spectrum **330**. Each Fabry-Pérot filter **222** in the filter array **220** that passes a different wavelength band provides a signal to produce other points on the radiance spectrum **330**. Accordingly, a snapshot of the output from the spectral sensor **125** gives the radiant intensity for the bandpass of each Fabry-Pérot filter **222** and can be used to generate the radiance spectrum **330** for a scene viewed by the camera **240**. Additional signal processing can be used to improve the resolution of the radiance spectrum **330**, as described below, and detect the presence of a chemical component.

[0054] The example radiance spectrum **330** can be altered by the presence of a chemical component, such as a harmful gas. In the plot of FIG. **3** containing the radiance spectrum **330**, an absorption spectrum **340** of a harmful gas is also plotted. Presence of the harmful gas in the field-of-view of the camera **240** produces a dip **335** in the radiance spectrum **330** that would not be present in a reference spectrum **350** obtained for the field-of-view when the harmful gas is not present.

2.1 Fabry-Pérot Filter Structure

[0055] According to some implementations, each Fabry-Pérot filter **222** in the filter array **220** comprises an optical resonant cavity **410** that is formed between two parallel reflective mirrors **420** (which may be reflective surfaces), as illustrated in FIG. **4**. The wavelengths that are transmitted by the cavity **410** with low loss are wavelengths that have a zero node or near zero node in the electric field vector at essentially the mirror boundaries of the cavity. The transmission efficiency of the filter can be described by the quality factor (Q) of the resonant cavity **410** and depends on the reflectivity of the mirrors **420**. Higher mirror reflectivity provides better spectral resolution, as can be seen in the plots of transmission as a function of wavelength for different mirror reflectivities R in FIG. **5**.

[0056] Without being bound to a particular theory, the filter's transmission τ_r can be expressed as follows.

$$\tau_r = \frac{T^2}{(1-R)^2}\left[1 + \frac{4R}{(1-R)^2}\sin^2\left(\frac{2\pi\mu t\cos\theta}{\lambda}\right)\right]^{-1} \quad (1)$$

T is the transmission of each mirror **420**, R is the reflectance of each mirror **420**, μ is the refractive index of the material filling the cavity **410** between the mirrors **420**, t is the thickness or length of the cavity **410** between the mirrors **420**, λ is the wavelength of radiation incident on the filter, and θ is the incident angle of the radiation. Each Fabry-Pérot filter **222** can have flat, parallel, and smooth mirror surfaces when fabricated and the components of the cavity **410** preferably have negligible intrinsic absorption of the radiation. The reflectivities of these mirrors controls the bandpass of the filter, as shown in FIG. **5**.

2.2 Bragg Mirrors

[0057] According to some implementations, Bragg mirrors **420** are used to bound the top and bottom of the Fabry-Pérot cavity **410**. Bragg mirrors **420** can be formed by alternating thin-film layers of material having different optical properties (e.g., different refractive index values). In some cases, the alternating layers can be dielectric material (e.g., oxide and semiconductor or two different semiconductors). A risk with such alternating layers is the adhesion of the thin film layers to the substrate and to each other. Adhesion failure and delamination of the layers can degrade mirror reflectivity or even render the mirror unusable. The materials choices for the thin-film layers in the multi-layer Bragg mirror define the performance of the mirror and also the risk of delamination. Increasing the number of layers of high and low index materials increases the reflectivity of the Bragg mirror **420** but also increases the risk of delamination.

[0058] FIG. **6**A and FIG. **6**B show the calculated performance of two different designs of Bragg mirrors **420**. The high index material in the mirror stack is germanium and the low index material is zinc sulfide. The etalon material in the resonant cavity **410** is also germanium. FIG. **6**A illustrates the transmittance of a Fabry-Pérot filter **222** where a single pair of thin-film layers is used for each Bragg mirror **420**. Several plots are generated for different thicknesses of the germanium etalon in the cavity **410**. FIG. **6**B illustrates the transmittance of a Fabry-Pérot filter **222** where four thin-film layers (two pairs of layers) are used for each Bragg mirror **420**. The two-pair mirror has a narrower passband to provide finer spectral resolution.

2.3 Sensor Resolution

[0059] FIG. **7** shows multiple plots generated from a modeling study to evaluate spectral resolution of spectrometer that uses the spectral sensor **125**. The plots reveal tradeoffs between the spectrometer's resolution and the number of different Fabry-Pérot filters **222** used in the spectral sensor **125** and the spectral bandpass of the filters **222**. The row labeled "A" shows the sensor's spectral resolution based on the two-pair mirror design of FIG. **6**B with a 95% reflectivity (R=0.95) of the cavity mirrors **420**. The sensor's spectral resolution improves (along with accuracy of detecting a reference sarin spectrum) when the number of Fabry-Pérot filters **222** at different bandpass wavelengths increases in the sensor. With only 10 filters of different bandpass wavelengths, the sensor's spectral reconstruction depends primarily on the sampling of the spectrum by the sensor's overall spectral sampling function. With 20 or more Fabry-Pérot filters **222** having different passbands, the spectral reconstruction depends more on the passband of the individual Fabry-Pérot filters **222**. With a mirror reflec-

tivity R=0.95 there is little improvement in the sensor's spectral resolution when increasing the number of filters above 20 and not much improvement when increasing the number of filters from 50 to 100 or more.

[0060] Increasing the reflectivity of the mirrors **420** decreases the widths of the passbands of the Fabry-Pérot filters **222** and increases the spectral resolution of the spectral sensor **125**, as can be seen in the rows of plots labeled "B" and "C" in FIG. **7**. The mirror reflectivities are increased to R=0.98 (row "B") and R=0.99 (row "C"). The increase in mirror reflectivity increases the measurement fidelity of the spectral sensor **125**. However, since the bandwidth of each Fabry-Pérot filter **222** is reduced there is also a decrease in the number of photons that reach the detector and an associated reduction in signal to noise ratio (SNR). The tradeoff between sensor resolution and SNR may impact the overall sensor design.

3. Grayscale Lithography and Cavity Fabrication

[0061] Initial considerations for fabricating the filter array **220** included defining a fabrication process and identifying the materials that could be brought into a fabrication facility and used to create the filter array. There are significant constraints on materials since many materials may be incompatible with the other work that is done in the fabrication facility and can negatively impact fabrication facility operations. Germanium and zinc sulfide can be used to fabricate the Fabry-Pérot filter **222** without deleterious effects on other fabrication facility operations where the filter arrays would be made. However, other fabrication facilities may tolerate other materials, and the invention is not limited to only germanium and zinc sulfide material for constructing the Fabry-Pérot filter **222**.

[0062] Several processes such as grayscale photolithography and etching were developed in order to fabricate the final Fabry-Pérot filter array **220**. Much of the process development was carried out on inexpensive and readily available silicon wafers on which there was deposited an additional germanium layer. This germanium layer was processed in the same way that the germanium cavity **410** would be processed in the final filter array **220**. FIG. **8** is a scanning electron microscope (SEM) image showing a cross section of an example wafer having about three microns of germanium **810** deposited on a silicon wafer **805**. A Wordentec e-beam deposition tool created the 3.1-micron-thick amorphous Ge layer on the silicon test wafer shown in FIG. **8**.

[0063] Grayscale lithography has been used to create complex features in silicon using a microelectronic fabrication process. FIG. **9** and FIG. **10**A through FIG. **10**D illustrate grayscale photolithography for generation of step heights in a photoresist **910** deposited on a substrate **905**. A mask **1020** having different features sizes is used to expose the photoresist **910**. The step heights generated in the photoresist **910** can later be transferred to different etch depths in the underlying substrate **905** by an etching process (e.g., reactive ion etching).

[0064] FIG. **9** is an overview of grayscale photolithography. A first mask **920** has large feature sizes and openings between features that are larger than the resolution limit for the exposing wavelength and optical stepper. Accordingly, patterns on the first mask **920** are reproduced in the photoresist **910** with high fidelity. FIG. **9** also shows masks **922**, **924** with grating patterns where the feature sizes are smaller than the resolution limit for the exposing wavelength and optical stepper used to "pattern" the photoresist **910**. In these cases, the masks **922**, **924** create aerial images of uniform intensity. The fine features on the masks **922**, **924** cannot be transferred to the photoresist **910** with high fidelity. The uniform aerial image is created by filtering out all of the higher order image components in the transform plane of the optical path of the stepper tool. Only the zeroth order of the illumination is used, and all of the modulation structure of the image is lost to create an even spatial illumination. Now, the intensity of the illumination depends only on the fill factor of the grating pattern on the mask. At these very small feature sizes, the mask acts like a uniform neutral density filter where the optical density of the filter is proportional to the grating fill factor used on the mask. The uniform intensity of the aerial image defines the relative exposure dose over an area in the resist **910** that corresponds to an area of the grating pattern on the mask. The exposure dose determines the thickness of the photoresist **910** after developing the photoresist. The different photoresist thicknesses represent different step heights.

[0065] FIG. **10**A through FIG. **10**D illustrate further details of grayscale photolithography. For the illustrated example, a germanium etalon layer **1015** (which can be used for a Fabry-Pérot cavity) is deposited on a silicon wafer (substrate **905**) and covered with a photoresist **910**. A portion of the resulting structure is shown in FIG. **10**A. The photoresist **910** is then exposed (FIG. **10**B) in an optical stepper using a grayscale mask **1020** having different grating or grid patterns **1031**, **1036** on the mask with feature sizes below the resolution limit of the optical stepper. For the illustrated example, there are six patterns on the mask with different fill factors. Pattern **1031** has the lowest fill factor, transmitting a higher optical dose (indicated by the light shading) into the photoresist **910**. Pattern **1036** has the highest fill factor, transmitting a lower optical dose (indicated by darker shading) into the photoresist **910**. To simplify the illustration, FIG. **10**B does not show the lenses of the optical stepper between the grayscale mask **1020** and photoresist **910** that would be present during exposure.

[0066] The resist is subsequently developed, resulting in the structure shown in FIG. **10**C. For the highest dose, a depression **1041** (e.g., a hole or trench) is formed in the photoresist **910** and may extend all the way to the germanium etalon layer **1015**. The lower doses may not clear the resist, resulting in different step heights of resist from the first depression **1041** to the sixth depression **1046**.

[0067] The wafer can then be subjected to an etching step (e.g., an anisotropic reactive ion etch) that etches the photoresist **910** and the germanium etalon layer **1015** at similar rates (e.g., etching rates within 20% of each other). The etching can transfer the step heights in photoresist **910** to step heights in the germanium etalon layer **1015**, resulting in the structure illustrated in FIG. **10**D. The photoresist **910** can be stripped from the wafer so that subsequent processing steps can be carried out (e.g., steps to deposit a mirror over the etalon layer **1015**).

[0068] For the illustrated example, the first four depressions **1041-1044** in the photoresist **910** are deep enough to result in etching of the underlying germanium etalon layer **1015**. The first depression **1041** in the photoresist may lead to complete removal of the germanium etalon layer **1015**, forming a void **1051**. Depressions **1042**, **1043**, **1044** result in partial etching of the germanium etalon layer **1015**, forming

germanium etalons **1052**, **1053**, **1054** having different thicknesses. These etalons can be used for Fabry-Pérot filters **222** having different passbands. By using the grayscale process, etalons for Fabry-Pérot filters **222** having different passbands can be fabricated on a same substrate using a single exposure and a single etching step.

3.1 Example Grayscale Mask for Fabricating Germanium Etalons

[0069] An example mask was used for initial fabrication of germanium etalons of different thicknesses using grayscale photolithography. SPR 220 Novalac resist is a suitable photoresist **910** for grayscale photolithography and etching of the germanium etalon layer **1015**.

[0070] The example mask includes multiple features in a test block for creating different etch depths in a germanium etalon layer on a silicon wafer, as described in connection with FIG. **10**A through FIG. **10**D above. FIG. **11**A illustrates a test block **1100** that includes an array of 500-micron×500-micron grating areas **1110** each having different grating patterns that are designed to provide controlled constant illumination across corresponding areas in the photoresist and to expose the photoresist with different doses. There are 375 different grating areas **1110** in the illustrated test block **1100**. FIG. **11**A also shows further details of the pattern in two grating areas **1110**. The grating areas **1110** have different grating pitches "P" (indicated in nanometers along two sides of the test block **1100**) and different fill factors (indicated as percentage values along top and bottom edges of the test block **1100**). The enlarged illustrations in FIG. **11**B and FIG. **11**C show a portion of the small-scale structure within each grating area **1110**. The grating areas **1110** in each row have the same pitch and the fill factor is varied across the row. The width of the grating lines **1115** in each grating area **1110** can be obtained by multiplying the pitch for the row times the fill factor for the column.

[0071] As described above, the fill factor for a pattern on the mask controls the amount of uniform illumination that exposes the photoresist **910** on the wafer. The grating areas **1110** with smaller fill factors provides the most illumination and higher exposure dose in the photoresist **910**. The higher dose results in a thinner layer of photoresist **910** after development. The grating areas **1110** with higher fill factors have less open area and transmit less light. Their corresponding exposed areas in the photoresist **910** have a thicker remaining layer of photoresist **910** after development. Since the photoresist acts as a destructible mask during etching, the etch chemistry works through the photoresist layer and begins to etch the germanium layer. The thinner photoresist etches through more quickly than the thicker photoresist, and the etch starts etching the germanium sooner under the thinner photoresist than under the thicker photoresist. Thus, the thinner photoresist results in a deeper etch depth and thinner germanium etalon **1052** and the thicker photoresist results in a shallower etch depth and thicker germanium etalon **1054**, as can be seen in FIG. **10**D.

[0072] FIG. **12** shows a visible camera image of an array of germanium etalons fabricated in a germanium layer on a silicon wafer using grayscale photolithography and the example mask having the test block **1100** of FIG. **11**. The enlarged images are SEM images of a germanium etalon fabricated from one of the grating areas **1110** (having a pitch of 875 nm, line width of 481 nm, and 55% fill factor). The highest resolution SEM image shows a smooth surface of the etalon (at the resolution of the SEM) and also shows a step height (etch depth) of 1.8 microns, meaning that the remaining etalon thickness is about 1.3 microns.

[0073] An FTIR microscope is a useful tool for characterizing the photolithography results and measuring the step heights (equivalent to etch depths) in the germanium etalon layer **1015**. The FTIR microscope can be set up for reflectance measurements but can also be used for transmission measurements. Since the silicon carrier wafer does not transmit the entire 8- to 12-micron spectral range, the reflectance measurements are a suitable way to evaluate the properties of the germanium etalon layer **1015** on the silicon substrate. Germanium has a relatively high refractive index (n~4 at these wavelengths) and the large index change between air and germanium creates a large surface reflection. A weaker surface reflection occurs at the germanium-silicon interface (n~3.42 for silicon at these wavelengths). These surface reflections create a weak interferometric effect that modulates the transmission intensity that is described by EQ. 1. The FTIR microscope is used to measure the reflectance r_r of the germanium etalon layer **1015** as a function of wavelength. The transmission through the germanium etalon layer can be approximated by subtracting the reflectance from 1 ($\tau_r=1-r_r$).

[0074] FIG. **13** shows a plot of the transmission (derived from $1-r_r$) of the germanium layer. FIG. **13** also shows a fit to the data using EQ. (1) with free parameters for the mirror (surface) reflectivity and the thickness of the germanium layer. In this case the mirror reflectivity was 0.11 and the germanium layer thickness was 3.15 microns. The asterisks mark the expected peak transmission positions for the layer thickness.

[0075] FIG. **14** shows measurements of reflectance as a function of wavelength for multiple germanium etalons having different thicknesses. The etalons were fabricated from grating areas **1110** in the mask of FIG. **11**A along the 575-nm-pitch row having different fill factors (from 22% to 80%). Also plotted are fits of the curves to EQ. (1). The mirror reflectivity R for EQ. (1) is held constant at 0.11 for the plots and the thickness t varied to obtain a fit to the measured data. Values of germanium etalon thickness t obtained from the fits to these measurements are plotted in FIG. **15** as a function of the corresponding fill factors for the measurements. The plot of FIG. **15** demonstrates that the germanium etalon thickness can be controlled by changing the fill factor of a grating pattern on a grayscale photomask that has sub-resolution-limit feature sizes.

3.2 Grayscale Photolithography Considerations

[0076] FIG. **15** also illustrates some issues to consider when using grayscale photolithography to form etalons for Fabry-Pérot filters **222**. At the higher fill factors (above ~0.6) the height of the germanium layer after processing is the same as the initial height (i.e., the germanium layer is not etched). At the higher fill factors there is insufficient dose in the photoresist **910** to allow removal of enough photoresist **910** during development. The subsequent etch process never penetrates through the photoresist **910** to reach the germanium etalon layer **1015** (as is the case for depressions **1045**, **1046** in FIG. **10**C). At low fill factors (below~0.2), the dose is so high that the photoresist **910** is too thin (or completely removed) after development. In this case the etch starts on the germanium etalon layer **1015** very early and completely

etches through the germanium by the end of the etch step (as is the case for depression **1041** in FIG. **10**C).

[0077] The data of FIG. **15** also indicates a process window for the fabrication of the germanium etalons. If the filter array **220** of the spectral sensor **125** (referring again to FIG. **1**) is to have 100 different bandpasses in the array, then 100 different germanium etalon thicknesses are to be fabricated. In first order (n=1 node between cavity mirrors), with larger separation between transmission peaks (larger free spectral range) all of the etalons for the Fabry-Pérot filters should have thicknesses between 1 micron and 1.5 microns, or between approximately those values. The fill factors for the grating patterns on the mask that correspond to those thicknesses are roughly between 0.35 and 0.39, which would mean control of the fill factor to better than 0.0004 per filter. Second order (n=2 nodes between cavity mirrors) has a smaller free spectral range but has a larger fill factor window from about 0.43 to 0.52. This would mean a precision of 0.0009 in the fill factor control to get 100 different wavelengths. Such sensitivity to fill factor is a fabrication challenge.

4. Fabrication of Fabry-Pérot Filter Arrays

[0078] A fabrication process having a suitable probability of success for fabricating arrays of Fabry-Pérot filters **222** is described. The process uses Ge substrate wafers. The fabrication process is compatible with processing in the microelectronics laboratory, which limits techniques and materials that can be used for fabrication of example Fabry-Pérot filters. Fabrication of the Fabry-Pérot filters using other facilities may permit use of wafers comprising other semiconductor materials (e.g., silicon, indium phosphide, gallium arsenide, etc.) along with use of other materials to form the Fabry-Pérot filters.

[0079] FIG. **16**A and FIG. **16**B show an elevation view (FIG. **16**A) and exploded view (FIG. **16**B) of an example Fabry-Pérot filter array **220**. The exploded view shows the different layers and structures involved in the fabrication process. To aid illustration, the layer thicknesses are not to scale. The filter array fabrication process is based on working directly on a germanium wafer **1610**, e.g., 200 mm germanium wafers. These wafers are electronic grade and are compatible with the fabrication facility to reduced concerns about introducing contamination into the facility.

4.1 Fabrication of High Reflectivity Bragg Mirrors and Filters

[0080] In a first step, dielectric layers for first Bragg mirrors **1620** were deposited on one 200 mm silicon test wafer and three 200 mm germanium wafers. Germanium and zinc sulfide are used for the dielectric layer of the Bragg mirrors **1620**. These layers can be deposited by chemical vapor deposition or sputtering.

[0081] The silicon wafer is used as a representative wafer of the lot for elemental analysis to detect the presence of contaminants. Elemental analysis showed high levels of gold contamination, unacceptable for the facility. Further observations indicated that the gold contamination came from dust and surface transfer as the wafers were repackaged. The wafers were cleaned by "scrubbing" the wafers with a very fine calcium oxide polishing compound using a chemical mechanical polishing (CMP) step to remove the surface contamination. One of the cleaned germanium wafers was sent for elemental analysis. The gold contamination on the germanium wafer was measured to be $<50\times10^{10}$ atoms/cm^2, which was acceptable for further processing.

[0082] After the first Bragg mirrors **1620** were formed, a germanium etalon layer **1015** was deposited on the wafers and etched to different thicknesses using the grayscale photolithograpy process described above. Second Bragg mirrors **1622** were then formed over the germanium etalon layer **1015** to define the Fabry-Pérot filters **222** having different bandpasses in the filter array **220**.

4.2 Fabry-Pérot Filter Array

[0083] FIG. **17** shows the layout of the filter array **220** having 24×32 Fabry-Pérot filters **222**. The grayscale in the drawing indicates the line-space ratio of the corresponding grating patterns on a grayscale photomask that would be used to form different etalon thicknesses for the Fabry-Pérot filters **222**. There are edge filters **1722**, **1724** located around the outside edge of the filter array **220** that are used for alignment. The corner filters **1724** shown in the lighter gray all have the same thickness that is designed to transmit 10.6-micron light. The edge filters **1722** with the darker tone are designed to transmit 8.6-micron light. These edge filters **1722**, **1724** can show up as alignment features by selective illumination of the edge filters. For example, 10.6-micron illumination shows the corner filters **1724**, whereas 8.6-micron illumination shows the edge filters **1722**. The 8.6-micron light is selected in this example because that wavelength is at the edge of the silicon transmission, so silicon can be used as a filter to show the edges of the filter array **220**.

[0084] With the outer edge filters **1722**, **1724** used for alignment, the remaining 22×30 filters are used for the different Fabry-Pérot filters **222** in the filter array **220**. There are 660 Fabry-Pérot filters **222** in the interior region but it is not necessary to have that many different wavelengths, as described in connection with FIG. **7** above, and it is not practical to try to control the grayscale lithography to that precision. Instead, there are 132 different gray levels, and each gray level appears 5 times in the filter array **220**. The different Fabry-Pérot filters **222** can be arranged in a pseudo-random pattern in the filter array **220**. This random pattern is used to mitigate spatial inhomogeneity across the illumination of the detector array **210**. The Fabry-Pérot filters **222** are designed to operate in second order to utilize a larger process window in the grayscale photolithography process. The etalon thicknesses of the Fabry-Pérot filter cavities vary between 1.84 and 3.16 microns with a 0.01-micron difference between steps. This range of etalon thicknesses nominally provides 132 different passbands across a spectral range from 7.36 microns to 12.64 microns.

[0085] In some implementations, the different Fabry-Pérot filters **222** can be arranged in a pre-determined pattern (e.g., in a Bayer-type or other deterministic spatial pattern) across the filter array **220**. The spectral sensor **125** can be thought of as a devices that maps spectral information in a field-of-view to a two-dimensional data matrix that represents a spectral fingerprint of the field of view, similar to the way in which a digital camera maps optical and spatial information to a two-dimensional data matrix that represents an optical image of the field-of-view. Accordingly, machine-learning processes (e.g., artificial intelligence applications) may be used to process the spectral two-dimensional data matrix to

improve detection of spectra of interest (such as spectra of harmful chemical gases). Strategically grouping and locating spectral bands across the sensor array may help a machine-learning process identify a spectrum of interest and/or distinguish the spectral signature from background clutter.

4.3 Example Grayscale Mask Layout

[0086] FIG. **18** shows the layout for a die **1810** on an example grayscale mask used to pattern filter arrays **220** like those of FIG. **17**. A Canon i-line stepper, used for grayscale photolithography, has a field size up to 50 mm×50 mm square. Up to the entire field size can be used for a single exposure. The die **1810** on the mask is used to create multiple filter arrays that match different detector arrays and can also provide arrays for testing purposes. For the example mask, there are grating areas **1820** to pattern four 24×32 filter arrays in the die **1810** where each Fabry-Pérot filter **222** in the array has a 400 micron×400 micron square size. The die **1810** also includes 32 smaller grating areas **1830** for patterning 24×32 filter arrays where each Fabry-Pérot filter **222** in the array has a 60 micron×60 micron square size. The die **1810** further includes a test block **1840**, shown in further detail with enlarged views. Each element of the test block **1840** represents a different two-dimensional grid pattern **1850** with different x and y fill factors. The two-dimensional features (rectangles) of the grid patterns **1850** have more process latitude for the grayscale process than grating lines for determining the photoresist exposure doses. Consequently, grid patterns **1850** were used to pattern the filter arrays **220**.

4.4 Anti-Reflection Coating

[0087] One silicon wafer and one germanium wafer, each having the stack of the first high reflectivity Bragg mirror **1620**, germanium etalon layer **1015**, and second high reflectivity Bragg mirror **1622**, were coated with a front anti-reflection (AR) coating **1640** (FIG. **16**A). These wafers demonstrated technical feasibility of the filter arrays **220**. The front AR coating **1640** can significantly reduce losses due to surface reflections at the high index germanium front surface.

5. Filter Testing

[0088] Using grayscale photolithography and the above-described fabrication processes, multiple filter arrays **220** having Fabry-Pérot filters **222** and test filters from the test block **1840** were fabricated on a silicon wafer and a germanium wafer. The silicon wafer was used as a trial of the fabrication process. Once the initial FTIR measurements of the silicon wafer were completed, the germanium wafer could be used to fabricate the filter arrays **220**. The germanium Fabry-Pérot filter arrays **220** were evaluated as follows.

[0089] Two different measurement setups were used to evaluate the filter arrays **220**. The first measurement was to look at the filter in the longwave infrared using a FLIR Boson® microbolometer camera, available from Teledyne FUR of Wilsonville, Oregon. The filter array **220** was positioned in the field-of-view of the camera. The camera was used with its regular lens. An additional 1-inch diameter, 1-inch focal length lens was used between the filter array **220** and the camera to transfer the image of the filter array **220** to the camera's detector array. Images were recorded of the filter array **220** with and without additional back illumination. A bandpass filter (center wavelength 10 microns with 0.5 micron full-width-half-max value) was used in the optical path. Additionally, an FTIR microscope was used to measure the optical properties of the filter array **220** in both reflectance and transmission modes.

[0090] FIG. **19** shows an image of Fabry-Pérot filters **222** in the test block **1840** that was recorded using the Boson® LWIR camera. The test block **1840** was illuminated from the back using a high temperature Globar source. One row of the filter array is not shown because the image field of the camera was limited by the size and focal length of the 1-inch diameter transfer lens. However, all of the squares from the 10% fill factor row were overexposed and the etalon layer **1015** was etched off of the wafer. Complete removal of the etalon layer is also observed for the 20% fill factor row in which the first **4** (and faint 5th) squares are visible.

[0091] FIG. **20**A through FIG. **20**C show images of filters **222** in the test block **1840** recorded with the FLTR Boson® camera **2030** and no additional illumination. FIG. **20**A shows the measurement setup, including the position of the transfer lens **2010** with respect to the filter array **220**. The 10-micron bandpass filter **2020** is also shown. FIG. **20**B shows the passive thermal image of the array with the histogram of recorded intensities. The 10-micron bandpass filter **2020** is removed from the setup for the data of FIG. **20**B. FIG. **20**C shows the image with the 10-micron bandpass filter **2020** between the transfer lens **2010** and the camera **2030** together with the histogram. The changes in the images and histograms show the wavelength dependence of the reflectance on the different filter elements. The histograms show much more intensity in the image with the bandpass filter than without. This is the result of the thermal radiance from the camera **2030** being reflected back to the camera by the bandpass filter **2020**. Much of the radiance from the camera **2030** that is not transmitted through the bandpass filter **2020** is reflected back to the camera and detected.

[0092] The second measurement setup uses the FTIR microscope to evaluate the Fabry-Pérot filters. FIG. **21**A illustrates parameters of the test array block. The number within each entry of the matrix gives the relative illumination intensity (normalized to 1) passed by each test grid pattern **1850**. Zero fill factor would correspond to an illumination intensity of 1, whereas 100% fill in x and 100% fill in y would correspond to zero illumination intensity passed by the grid pattern **1850**. The highest illumination intensity occurs for 10% fill factors in x and y. The lowest illumination intensity occurs for 100% fill factor in x and 90% fill factor in y. The shading in the matrix indicates the useful exposure range for making etalons of different thicknesses for the Fabry-Pérot filters **222**. The middle shading **2110** in the middle of the matrix (for relative intensities between 0.59 and 0.89) indicates areas where the photolithography and etch process creates different etch depths in the etalon layer **1015** that produce passbands at different wavelengths. Lower shading **2120** for lower fill factors indicates overexposure of the resist and excessive removal of the etalon layer **1015**. Upper shading **2130** for higher fill factors indicates exposure intensities that are too low to impact the etalon layer (the etalon layer is unetched and the filters all have the same spectral profile, upper plots in FIG. **21**B).

[0093] FIG. **21**B shows the measured spectra of the filters. The spectra are measured in reflectance but are shown as transmission (derived from reflectance as transmission=1−reflectance). The spectra at the top of FIG. **21**B all have a feature at 10.6 micron and are from underexposed photoresist and an unetched etalon layer, corresponding to the higher fill factors in FIG. **21**A.

[0094] The spectra shown in FIG. **21**B can be rearranged in order of the transmission peak for comparison to the target filter transmission functions that are plotted in FIG. **3**. This comparison is shown in FIG. **22**A and FIG. **22**B. The plot in FIG. **22**A (reproduced from FIG. **3**) shows the targeted transmission functions (for 25 filters not 132) while the plot in FIG. **22**B shows transmission functions actually produced with filters fabricated in the test block **1840**. Although the measured spectra look like the targeted spectra, some of the transmission spectra show additional spectral features at longer wavelengths. Also, as noted above, these FTIR measurements are based on reflectance measurements, not transmission measurements.

6. Discussion of Test Filter Results

[0095] To understand the origins of the additional spectral features in FIG. **22**B, consider the results from the measurement of germanium layers (no Bragg mirrors) on silicon shown in FIG. **13**. These measurements are shown in the top graph "A" of FIG. **23**. In FIG. **23** (graph A), the thickness that was derived from the fit to the data of FIG. **13** is used to predict what the filter's transmission curve would look like if there were 98% reflective Bragg mirrors on the top and bottom of the Fabry-Pérot cavity. The resulting curve **2310** shows the spectral behavior that the filter is designed to achieve. The middle panel of FIG. **23** (graph B) shows what was actually observed for the reflectance measurement cast as transmission and there are a number of additional peaks observed in reflection measurement. The origins of these additional peaks can be understood in terms of the design specification and initial Bragg mirror fabrication.

[0096] The high reflectivity Bragg mirrors were supposed to be deposited onto two germanium wafers and one silicon wafer. Each stack was supposed to terminate in a low-index ZnS layer. Generally, however, creating a high reflectivity mirror and terminating with a low index layer are mutually exclusive. To compensate, the high reflectivity mirror may have included an additional quarter wave layer of germanium. The full 3.11-micron layer was deposited on the resulting stack. The wafers were then subjected to the photolithography and etch processes designed for the 3.11-micron layer. However, there was an additional high index quarter wave element in the design, so the process did not operate in the target second order but in the third order, which had a smaller free spectral range.

[0097] The operation in third order is indicated in FIG. **23**. The top panel of FIG. **23** (graph A) is derived from FIG. **13** and shows the transmission derived from reflectance for the germanium on silicon features. Also shown in the top panel is the transmission curve **2310** that would be expected for the same thickness of germanium in a cavity between two high reflectivity mirrors. The top plot shows the expected free spectral range.

[0098] The middle plot of FIG. **23** (graph B) shows the transmission derived from the measured reflectance for one of the under-exposed grid patterns **1850** in the test block **1840**. The thickness of the corresponding etalon layer was expected to be the germanium thickness deposited using the Wordentec tool. This plot shows more transmission peaks than would have been expected for the 3.11-micron thick germanium layer. The bottom plot of FIG. **23** (graph C) shows the calculated transmission spectrum for a 3.75-micron thick germanium layer. This calculation looks more like what is observed in the measurement.

[0099] The difference between the 3.75-micron layer that produces the calculated spectrum and the intended 3.11-micron layer is 0.64 microns. The thickness of the quarter-wave layer of germanium (refractive index ~4) at a 10-micron center wavelength would be 10/16 micron, or 0.625 micron, which is consistent with the difference between the intended germanium thickness (3.11 microns) and the germanium thickness that reproduces the observed spectrum (3.75 microns). The 0.625-micron discrepancy and difference in transmission spectra can be attributed to the germanium layer deposited on top of the Bragg mirror stack in order to make a functioning high-reflectivity Bragg mirror. The additional spectral features that are observed in FIG. **22**B are the result of the additional germanium thickness. The spectral features can be suppressed from the spectra of other devices by adjusting the layer thicknesses and/or compositions accordingly. For example, the etalon layer could be reduced in thickness to compensate for the quarter-wave germanium layer added to the Bragg mirror stack. Alternatively or additionally, the composition of the etalon layer can be changed to change its refractive index.

[0100] As discussed above, FIG. **23** presents transmission as "transmission derived from reflectivity" since reflectivity is measured using the FTIR microscope and transmission is then calculated assuming that there is no absorption or scattering in the Fabry-Pérot filter. Additional measurements were made with the FTIR microscope reconfigured to directly measure filter transmission.

[0101] In order to make sure that the reconfigured FTIR microscope was functioning as expected to measure transmission spectra, the instrument was used to measure the transmission spectrum of a polystyrene film. Polystyrene film is a widely used standard for frequency and intensity calibration of FTIR instruments. FIG. **24**A and FIG. **24**B show the reference and measured polystyrene spectra, respectively. The match between these spectra show that the instrument is working as expected. A Fabry-Pérot filter **222** was then measured in transmission using the FTIR microscope and the result is shown in FIG. **24**C. The initial results showed very little transmission over the 8- to 12-micron range and very little of the expected filter bandpass. As a sanity check, the transmission of a Thor Labs **10** bandpass filter was measured. The filter had a center wavelength of 10 micron and a full-width-half-max value of 0.5 micron.

[0102] FIG. **25** shows a comparison of the measured transmission and reflectance spectra for two of the Fabry-Pérot filter elements fabricated from two grid patterns **1850** in the test block **1840**. One grid pattern **1850** has 50% x/80% y fill factors and the other pattern has 30% x/50% y fill factor. For both of these cases, the target peaks show very strong dips or notches in reflectance (suggesting high transmittance at those wavelengths). For the 30%/50% filter the reflectance notch is the strongest feature in the reflectance spectrum. However, the transmission spectra do not show significant transmission peaks corresponding to the reflectance notches. Instead, each spectrum shows a very small transmission peak at the reflectance minima. In both spectra

there a numerous corresponding reflectance notches and associated transmission peaks, and the targeted filter peaks are impacted the most. The suppression of the target peaks may be due to absorptive adhesion layer(s) in the Bragg mirror stack.

[0103] The Fabry-Pérot filters show weak transmission in the 8-micron to 12-micron range. FIG. **26** presents the results of the transmission measurements made with the FTIR microscope in a way that better indicates the targeted spectra shown in FIG. **3**. The results indicate that grayscale photolithography can be used to create different etalon thicknesses for a working filter array **220**.

7. Filter Spacing and Signal Processing

[0104] The inventor has recognized and appreciated that spectral resolution of a spectrometer that includes a spectral sensor **125** can be improved by spacing the passbands of the spectral sensor **125** judiciously and using appropriate signal processing techniques. For example, instead of completely separating the passbands of the Fabry-Pérot filters **222** such that their passbands do not overlap by any significant amount, the passbands are located such that adjacent passbands overlap by an appreciable amount. In some implementations, the adjacent passbands are spaced such that a crossing of the adjacent passbands or transmission functions, corresponding to the two adjacent transmission functions, lies at a value no less than 10% of peaks of the two transmission functions.

[0105] FIG. **27** shows a plurality of such overlapping transmission functions corresponding to Fabry-Pérot filters **222** in a filter array **220**. There can be at least five or ten such overlapping transmission functions for a filter array **220**. In the illustration, there are approximately 29 evenly-spaced transmission functions covering the wavelength range from 8 microns to 12 microns. The transmission functions overlap such that a crossing **2715** of two adjacent transmission functions **2710**, **2720** lies at a value of about 65% of the peaks of the two adjacent transmission functions. Other crossing values are also possible. In an implemented device, the transmission functions can overlap such that a crossing **2715** of two adjacent transmission functions **2710**, **2720** lies at a value in a range from 5% to 95% of the peaks of the two adjacent transmission functions. In some implementations having multiple transmission functions, the crossings **2715** need not all be at a same value of the transmission functions. There can be crossings **2715** of different values for different pairs of adjacent transmission functions. The crossings **2715** can be determined through filter design (e.g., determining a center wavelength for a filter, which is dependent on spacing or optical path length between the filters two mirrors, and determining a passband for the filter, which is dependent on mirror reflectivity or number of Bragg layers).

[0106] Although the functions are evenly spaced in the illustration of FIG. **27**, they need not be. In some cases, there can be unequal spacing between transmission functions in a filter array **220**. In some cases, some transmission functions may overlap by an appreciable amount (crossing at a 10% value or higher) and some transmission functions may not overlap by any significant amount (crossing at a 5% value or lower). In some cases, the crossing can at a value that is no less than 25%, no less than 50%, or even no less than 75%. There can be multiple transmission functions (e.g., at least 10) of the Fabry-Pérot filters **222** that are spaced apart such that the peak transmission wavelengths of the different optical filters are different from each other by a value that is at least 10% or more of the full-width half-maximum (FWHM) value for the transmission functions. In FIG. **27**, the FWHM value is indicated by a horizontal line with two arrows and the adjacent transmission functions are spaced apart such that their peak transmission wavelengths differ by and amount that is approximately 70% of the FWHM value of the adjacent transmission functions. When the FWHM value of adjacent transmission functions differ, the separation can be a percentage of the average value of the two FWHM values for the adjacent transmission functions.

[0107] In practical implementations, the transmission functions for the different Fabry-Pérot filters **222** may differ from each other (e.g., due to manufacturing variations that naturally occur in microfabrication processes). However, the Fabry-Pérot filter transmission functions can be measured and characterized to develop a spectrometer response function.

[0108] FIG. **28** shows simulated results of a measurement of a reference spectrum **2810** with a spectrometer having Fabry-Pérot filters **222** with overlapping transmission functions, like those illustrated in FIG. **27** but for a larger number of filters. The reference spectrum **2810** could correspond to the emission spectrum of a particular gas, for example. The raw, measured spectrum **2820** (where filter values are plotted as circles and interpolated with a continuous curve) barely resembles the reference spectrum **2810**. However, knowledge of the spectrometer's transmission functions can be used to deconvolve the measured spectrum **2820** and recover a deconvolved spectrum **2910**, shown in FIG. **29**. For easier visual comparison, the reference spectrum **2810** is plotted again in FIG. **29** and the deconvolved spectrum **2910** is offset in intensity.

[0109] Measurement and deconvolution of the measured spectrum **2820** can be understood as follows. The intensity value $[I]_i$ at a wavelength on the measured spectrum **2820** for each Fabry-Pérot filter **222** is an integral of that Fabry-Pérot's transmission function multiplied by the reference spectrum that is being measured. The subscript i indicates the Fabry-Pérot filter index. Each Fabry-Pérot filter samples some of the spectrum to either side of the Fabry-Pérot's FWHM values that can lie in at least one adjacent filter's transmission function. However, the weighting of the sampled spectral features will differ according to the filters' transmission functions. The deconvolution takes advantage of the sampling and different weighting when recovering the deconvolved spectrum **2910**.

[0110] Another way of considering the spectrometer response is as follows. The spectrometer samples light at any given wavelength with different weighting values by multiple filters. Accordingly, the spectrometer response at any given wavelength can be written as a response vector (which can be determined through filter calibrations). A set of response vectors for different selected wavelengths can be formed into a response matrix $[C]_{i,j}$ that is representative of the spectrometer response function. The subscript j indicates a wavelength index for the selected wavelengths.

[0111] Without being bound to a particular theory, the deconvolution process can be expressed as

$$[S]^*_j=[C]_{i,j}^{-1}[I]_i \tag{2}$$

where $[S]^*_j$ is the recovered, deconvolved spectrum **2910**, $[C]_{i,j}^{-1}$ is the inverse of response matrix $[C]_{i,j}$, and $[I]_i$ is the

raw measured spectrum **2820**. As can be seen in FIG. **29**, the deconvolution accurately recovers the reference spectrum **2810**.

8. Spectral Sensor Applications

[0112] The spectral sensor **125** can be used in different spectral sensing and diagnostic applications. FIG. **30** shows another low-SWAP spectrometer **3005** in which two spectral sensors **125-1**, **125-2** and a radiation source **3010** are configured to analyze a sample placed in a sample region **3020**. Radiation from the radiation source **3010** (e.g., an incandescent bulb) can travel to a reference spectral sensor **125-1**, which measures a reference spectrum indicative of spectral emission from the radiation source **3010**.

[0113] The radiation source **3010** can also emit radiation that travels to the sample region **3020** to illuminate a sample placed in the region. Radiation can pass through the sample and be detected by a second spectral sensor **125-2**. Absorption of the radiation by the sample can alter the spectrum from the radiation source **3010**. Comparison of the detected spectrum (obtained from the second spectral sensor **125-2**) with the reference spectrum (obtained from the first spectral sensor **125-1**) can reveal information about the material placed in the sample region **3020** (e.g., type or composition of gas or liquid). In some cases, radiation reflected by the sample may be analyzed instead of, or in addition to, radiation that passes through the sample. The configuration of the spectrometer **3005** can be modified (e.g., by rearranging the location of the second spectral sensor **125-2** with respect to the sample region **3020** and radiation source **3010** or adding a third spectral sensor) to detect radiation reflected from the sample.

[0114] In some cases, optical components **3030** can be included to direct radiation from the radiation source **3010** to the first spectral sensor **125-1** and/or to the second spectral sensor **125-2**. For example, guiding optical components can be used to guide and/or homogenize the radiation from the radiation source **3010**. The guiding optical components can be some combination of cylindrical, square, or polygonal shaped total internal reflectors, multimode waveguides, cylindrical, square, or polygonal shaped mirrors, conical mirrors, etc. In some cases, one or more lenses may be used in the optical assembly. As depicted, the distance between the spectral sensors can be no larger than 25 mm or 30 mm, though some devices may have a spacing between the spectral sensor that is no larger than 60 mm.

[0115] FIG. **31** depicts another configuration of a low-SWAP spectrometer **3105**, which can be the size of a pen. The spectrometer **3105** can be used to analyze a liquid sample **3108**. The device operates like that shown in FIG. **30** though the optical path between spectral sensors **125-1**, **125-2** is folded. An attenuated total reflectance (ATR) cell **3120** is placed at the fold in the optical path. The ATR optic **3120** can be a solid optical component (e.g., a conical-shaped or prism-shaped solid optic) for which light entering a first portion **3122** of a face of the ATR optic **3120** undergoes total internal reflection (TIR) in the ATR optic **3120** and exits a second portion **3124** of the face of the ATR optic **3120**. The radiation undergoing TIR is attenuated through evanescent optical fields that extend into the liquid sample **3108**. This attenuation alters the spectrum emitted from the radiation source **3010** and the altered spectrum is detected by the second spectral sensor **125-2**.

[0116] The low-SWAP spectrometer **3105** of FIG. **31** includes an on-board power source **3140** (e.g., one or more batteries) that is coupled to and powers an on-board controller **3150** (e.g., a microcontroller, microprocessor, digital signal processor, field-programmable gate array, or other signal processing device). The spectrometer **3105** can further include on-board memory (not shown) that is communicatively coupled to the controller **3150**.

[0117] For the configuration of FIG. **31**, the first spectral sensor **125-1** and second spectral sensor **125-2** can be formed on four different substrates (two for the first spectral sensor and two for the second spectral sensor). Alternatively, the first spectral sensor **125-1** and second spectral sensor **125-2** can be formed on two substrates (one substrate that includes both filter arrays and one substrate that includes both detector arrays).

[0118] The low-SWAP spectrometer **3005** of FIG. **30** can also be packaged to include an on-board power source that is operably coupled to and powers an on-board controller and on-board memory. A length L of the spectrometers **3105**, **3005** can be no longer than 50 mm in some cases or no longer than 100 mm in some cases. A width W or diameter of the spectrometers **3105**, **3005** can be no wider than 10 mm in some cases, no wider than 20 mm in some cases, no wider than 30 mm in some cases, or no wider than 50 mm in some cases. However, it is possible to package the spectrometer in assemblies having sizes larger than these values.

[0119] Though the above-described Fabry-Pérot filter arrays, spectrometers, and signal processing techniques are described mainly for a long-wavelength infrared region (from about 8 micron wavelengths to about 12 micron wavelengths), the apparatus and/or techniques can be implemented for other wavelength regions. For example, the apparatus and/or techniques can be implemented for visible wavelength regions or near-infrared wavelength regions.

[0120] Though the Fabry-Pérot filters, spectrometers, and signal processing techniques are described mainly for operation in transmission mode, the Fabry-Pérot filters and spectrometers can be operated in reflection mode as mentioned above. When operating in reflection mode, the filter spacing can be determined from the notches in the Fabry-Pérot filters' reflectivity functions. For example, the notch in a reflectivity function corresponds to a transmission peak in the transmission function, as indicated in FIG. **25**. The reflectivity function can be subtracted from 1 to obtain a transmission function for each filter, and the spacing expressed in terms of FWHM values of the resulting transmission functions. The signal processing can use a reflectivity response matrix for the spectrometer to deconvolve the measured spectrum instead of a transmission response matrix. The deconvolved spectrum can then be subtracted from 1 to obtain a transmission spectrum for further analysis.

[0121] Though the filter arrays **220** and detector arrays **210** are described as being formed on different substrates that are later aligned and packaged together, it is also possible to form the filter arrays **220** and detector arrays **210** on a same substrate. For example, a detector array can be fabricated first on a substrate and protected with an oxide layer or other layer that transmits radiation to be detected. The filter array can then be fabricated over the detector array on the same substrate, aligned to the detector array.

[0122] Spectral analysis performed on data collected with the spectral sensor **125** described above can further include

comparing a deconvolved measured spectrum with a background reference spectrum to determine the presence of absorption of the background reference spectrum at wavelengths that may indicate the presence of a chemical component. For example, the background reference spectrum can be obtained for a field-of-view when it is known that the chemical component is not present. The presence of the chemical component (such as a chemical gas) in the field of view can result in absorption of certain wavelengths in the reference spectrum. Subtracting the deconvolved measured spectrum from the reference spectrum can produce a difference spectrum that indicated the presence of the chemical gas.

9. Conclusion

[0123] While various inventive embodiments have been described and illustrated herein, those of ordinary skill in the art will readily envision a variety of other means and/or structures for performing the function and/or obtaining the results and/or one or more of the advantages described herein, and each of such variations and/or modifications is deemed to be within the scope of the inventive embodiments described herein. More generally, those skilled in the art will readily appreciate that all parameters, dimensions, materials, and configurations described herein are meant to be exemplary and that the actual parameters, dimensions, materials, and/or configurations will depend upon the specific application or applications for which the inventive teachings is/are used. Those skilled in the art will recognize or be able to ascertain, using no more than routine experimentation, many equivalents to the specific inventive embodiments described herein. It is, therefore, to be understood that the foregoing embodiments are presented by way of example only and that inventive embodiments may be practiced otherwise than as specifically described. Inventive embodiments of the present disclosure are directed to each individual feature, system, article, material, kit, and/or method described herein. In addition, any combination of two or more such features, systems, articles, materials, kits, and/or methods, if such features, systems, articles, materials, kits, and/or methods are not mutually inconsistent, is included within the inventive scope of the present disclosure.

[0124] Also, various inventive concepts may be embodied as one or more methods, of which an example has been provided. The acts performed as part of the method may be ordered in any suitable way. Accordingly, embodiments may be constructed in which acts are performed in an order different than illustrated, which may include performing some acts simultaneously, even though shown as sequential acts in illustrative embodiments.

[0125] All definitions, as defined and used herein, should be understood to control over dictionary definitions, definitions in documents incorporated by reference, and/or ordinary meanings of the defined terms.

[0126] The indefinite articles "a" and "an," as used herein, unless clearly indicated to the contrary, should be understood to mean "at least one."

[0127] The phrase "and/or," as used herein, should be understood to mean "either or both" of the elements so conjoined, i.e., elements that are conjunctively present in some cases and disjunctively present in other cases. Multiple elements listed with "and/or" should be construed in the same fashion, i.e., "one or more" of the elements so conjoined. Other elements may optionally be present other than the elements specifically identified by the "and/or" clause, whether related or unrelated to those elements specifically identified. Thus, as a non-limiting example, a reference to "A and/or B", when used in conjunction with open-ended language such as "comprising" can refer, in one embodiment, to A only (optionally including elements other than B); in another embodiment, to B only (optionally including elements other than A); in yet another embodiment, to both A and B (optionally including other elements); etc.

[0128] As used herein, "or" should be understood to have the same meaning as "and/or" as defined above. For example, when separating items in a list, "or" or "and/or" shall be interpreted as being inclusive, i.e., the inclusion of at least one, but also including more than one, of a number or list of elements, and, optionally, additional unlisted items. Only terms clearly indicated to the contrary, such as "only one of" or "exactly one of" or "consisting of," will refer to the inclusion of exactly one element of a number or list of elements. In general, the term "or" as used herein shall only be interpreted as indicating exclusive alternatives (i.e., "one or the other but not both") when preceded by terms of exclusivity, such as "either," "one of," "only one of," or "exactly one of." "Consisting essentially of," shall have its ordinary meaning as used in the field of patent law.

[0129] As used herein, the phrase "at least one," in reference to a list of one or more elements, should be understood to mean at least one element selected from any one or more of the elements in the list of elements, but not necessarily including at least one of each and every element specifically listed within the list of elements and not excluding any combinations of elements in the list of elements. This definition also allows that elements may optionally be present other than the elements specifically identified within the list of elements to which the phrase "at least one" refers, whether related or unrelated to those elements specifically identified. Thus, as a non-limiting example, "at least one of A and B" (or, equivalently, "at least one of A or B," or, equivalently "at least one of A and/or B") can refer, in one embodiment, to at least one, optionally including more than one, A, with no B present (and optionally including elements other than B); in another embodiment, to at least one, optionally including more than one, B, with no A present (and optionally including elements other than A); in yet another embodiment, to at least one, optionally including more than one, A, and at least one, optionally including more than one, B (and optionally including other elements); etc.

[0130] In the specification above, all transitional phrases such as "comprising," "including," "carrying," "having," "containing," "involving," "holding," "composed of," and the like are to be understood to be open-ended, i.e., to mean including but not limited to. Only the transitional phrases "consisting of" and "consisting essentially of" shall be closed or semi-closed transitional phrases, respectively, as set forth in the United States Patent Office Manual of Patent Examining Procedures, Section 2111.03.

What is claimed is:

1. A spectral sensor comprising:

a first substrate;

an array of optical filters formed on the first substrate, each optical filter having:

a first mirror formed on the first substrate;

a second mirror spaced apart from the first mirror and in optical communication with the first mirror; and

an etalon formed between the first mirror and the second mirror;

a second substrate; and

an array of detectors formed on the second substrate, the array of detectors in optical communication with the array of optical filters,

wherein the array of optical filters includes at least 10 optical filters for which the etalons of the 10 optical filters have different thicknesses such that the 10 optical filters have different transmission functions or different reflectivity functions, and

the etalons of the 10 optical filters having the different thicknesses are all etched from a same layer of material on the first substrate.

2. The spectral sensor of claim **1**, wherein:

the 10 different optical filters each have a transmission function with a peak transmission wavelength and a full-width half-maximum value of the transmission function;

the peak transmission wavelengths of the 10 different optical filters are different from each other by a value that is at least 10% of the full-width half-maximum value; and

each transmission function of the 10 different optical filters partially overlaps in wavelength with another transmission function of another optical filter of the 10 different optical filters.

3. The spectral sensor of claim **2**, wherein a partial overlap of two of the transmission functions comprises a crossing of the two transmission functions at a value no less than 10% of peak values of the two transmission functions.

4. The spectral sensor of claim **1**, wherein the first substrate and the second substrate are a same substrate.

5. The spectral sensor of claim **1**, wherein the 10 different optical filters each have a transmission function with a peak value in a range between 8 microns and 12 microns.

6. The spectral sensor of claim **2**, wherein a full-width half-maximum value of each transmission function is no larger than 0.5 microns.

7. The spectral sensor of claim **1**, wherein at least one optical filter in the array of optical filters is in optical communication with more than one detector in the array of detectors.

8. The spectral sensor of claim **1**, wherein the array of optical filters includes at least two optical filters that have a same transmission function or a same reflectivity function and the 10 different optical filters are located randomly in the array of optical filters.

9. The spectral sensor of claim **1**, further comprising an optical element to spatially homogenize radiation from a scene viewed by the spectral sensor, such that the spectral sensor does not image the scene.

10. The spectral sensor of claim **1**, wherein the same layer of material is formed from germanium.

11. The spectral sensor of claim **1**, wherein the first mirror is a multilayer Bragg mirror.

12. A handheld spectrometer comprising the spectral sensor of claim **1**, wherein the spectral sensor is arranged to receive radiation to be spectrally analyzed.

13. The handheld spectrometer of claim **11**, further comprising:

a controller in communication with the spectral sensor to receive signals from the array of detectors; and

a radiation source to deliver the radiation to a sample; and

a power source to provide power to the controller and to the radiation source.

14. The handheld spectrometer of claim **13**, further comprising an attenuated total reflectance (ATR) optic arranged in an optical path between the radiation source and the spectral sensor, wherein the ATR is configured to contact a liquid such that evanescent fields from the radiation passing through the ATR optic extend into the liquid.

15. The handheld spectrometer of claim **11**, wherein a length of the handheld spectrometer is no longer than 60 mm and a width of the handheld spectrometer is no wider than 30 mm.

16. The handheld spectrometer of claim **11**, wherein the spectral sensor is a first spectral sensor, the array of optical filters is a first array of optical filters, and the array of detectors is a first array of detectors, the handheld spectrometer further comprising a second spectral sensor arranged to receive radiation from the radiation source to produce a reference spectrum, the second spectral sensor comprising:

a third substrate;

an array of optical filters formed on the third substrate, each optical filter of the second array of optical filters having:

a first mirror formed on the third substrate;

a second mirror spaced apart from the first mirror an in optical communication with the first mirror; and

an etalon formed between the first mirror and the second mirror;

a fourth substrate; and

a second array of detectors formed on the fourth substrate, the second array of detectors in optical communication with the second array of optical filters,

wherein the second array of optical filters includes at least 10 optical filters for which the etalons of the 10 optical filters have different thicknesses such that the 10 optical filters have different transmission functions or different reflectivity functions, and

the etalons of the 10 optical filters having the different thicknesses are all etched from a same layer of material on the third substrate.

17. A method of making a spectral sensor, the method comprising:

illuminating a grayscale photomask to expose a photoresist and pattern an array of etalons for Fabry-Pérot filters, wherein the photoresist is deposited over an etalon layer on a substrate;

developing the photoresist such that the photoresist has at least 10 different thicknesses over the etalon layer; and

etching the photoresist and at least a portion of the etalon layer to pattern the array of etalons, wherein the array of etalons includes at least 10 etalons having different thicknesses.

18. The method of claim **17**, wherein the etching is a single processing step that etches both the photoresist and the etalon layer.

19. The method of claim **17**, further comprising:

depositing a mirror over the array of etalons to form an array of Fabry-Pérot filters that comprises 10 different optical filters, wherein

the 10 different optical filters each have a transmission function with a peak transmission wavelength and a full-width half-maximum value of the transmission function;

the peak transmission wavelengths of the 10 different optical filters are different from each other by a value that is at least 10% of the full-width half-maximum value; and

each transmission function of the 10 different optical filters partially overlaps in wavelength with another transmission function of another optical filter of the 10 different optical filters.

20. The method of claim **19**, further comprising:

optically coupling the array of Fabry-Pérot filters to an array of detectors.

* * * * *